2-deoxyglucose transiently inhibits yeast AMPK signaling and triggers glucose transporter endocytosis, potentiating the drug toxicity

Clotilde Laussel[#1], Véronique Albanèse[#1], Francisco Javier García-Rodríguez[&,1], Alberto Ballin[&,1], Quentin Defenouillère[1], Sébastien Léon[1,2]

Affiliations:

[#]: Equal contributions
[&]: Equal contributions
[1]: Université Paris Cité, CNRS, Institut Jacques Monod, F-75013, Paris, France.

[2]: Author for correspondence:

Sébastien Léon, PhD
Institut Jacques Monod
15 Rue Hélène Brion
75205 Paris cedex 13, France.
email: sebastien.leon@ijm.fr ; tel. +33 (0)1 57 27 80 57.

Running title:

Effects of 2-deoxyglucose on yeast AMPK signaling and endocytosis, and contribution to 2DG tolerance

Abstract

2-deoxyglucose is a glucose analog that impacts many aspects of cellular physiology. After its uptake and its phosphorylation into 2-deoxyglucose-6-phosphate (2DG6P), it interferes with several metabolic pathways including glycolysis and protein N-glycosylation. Despite this systemic effect, resistance can arise through strategies that are only partially understood. In yeast, 2DG resistance is often associated with mutations causing increased activity of the yeast 5'-AMP activated protein kinase (AMPK), Snf1. Here we focus on the contribution of a Snf1 substrate in 2DG resistance, namely the alpha-arrestin Rod1 involved in nutrient transporter endocytosis. We report that 2DG triggers the endocytosis of many plasma membrane proteins, mostly in a Rod1-dependent manner. Rod1 participates in 2DG-induced endocytosis because 2DG, following its phosphorylation by hexokinase Hxk2, triggers changes in Rod1 post-translational modifications and promotes its function in endocytosis. Mechanistically, this is explained by a transient, 2DG-induced inactivation of Snf1/AMPK by protein phosphatase 1 (PP1). We show that 2DG-induced endocytosis is detrimental to cells, and the lack of Rod1 counteracts this process by stabilizing glucose transporters at the plasma membrane. This facilitates glucose uptake, which may help override the metabolic blockade caused by 2DG, and 2DG export - thus terminating the process of 2DG detoxification. Altogether, these results shed a new light on the regulation of AMPK signaling in yeast and highlight a remarkable strategy to bypass 2DG toxicity involving glucose transporter regulation.

Author summary

In this article, we study the resistance to a drug named 2-deoxyglucose (2DG). 2DG is an efficient inhibitor of several metabolic pathways, particularly glycolysis which is of prime importance for tumor cell proliferation. Cancer cells but also cells from other organisms can develop various resistance strategies that only being unraveled. Here, using baker's yeast as a model organism, we document the resistance mechanism of a mutant lacking the arrestin gene *ROD1*, known to regulate nutrient transporter endocytosis. First, we show that 2DG triggers the endocytosis of many nutrient transporters. Mechanistically, 2DG leads to a transient inhibition of the AMPK signaling pathway, which in turn promotes the activation of Rod1, a pre-requisite for 2DG-induced endocytosis. Consequently, cells lacking Rod1 maintain various proteins at the plasma membrane including hexose transporters, the latter being essential for 2DG resistance. Hexose transporter stabilization at the cell surface may sustain glucose import and help cells cope with the 2DG-induced metabolic blockade, while also allowing 2DG detoxication.

67 # Introduction

68

69 2DG is a glucose analog which lacks a hydroxyl group in position 2, and mainly acts as a competitive
70 inhibitor of glucose metabolism [1]. As such, it competes with glucose for entry into cells and for its
71 subsequent phosphorylation by hexokinase, but is almost not further metabolized. This leads to the
72 intracellular accumulation of 2DG-6-phosphate, a toxic metabolite that inhibits glycolysis and thus leads to a
73 rapid depletion of ATP stores, and the activation of nutrient starvation-activated pathways such as 5'-AMP
74 activated protein kinase, AMPK [2]. Moreover, since mannose is the C2 epimer of glucose, 2-deoxyglucose is
75 also 2-deoxymannose and thus also interferes with mannose metabolism, notably inhibiting protein N-
76 glycosylation [reviewed in 3]. This causes a series of cellular effects, and triggers the onset of the Unfolded
77 Protein Response pathway to face the stress encountered by a defective glycosylation of proteins at the
78 endoplasmic reticulum, which is reportedly the main toxic effect of 2DG in some conditions [4].

79 The realization that many cancer cells display an aberrantly high glucose uptake and metabolism has led
80 to the idea that glycolysis inhibitors could be used to preferentially target and kill tumor cells [5]. This also
81 allowed the use of radiolabeled glucose derivatives, such as 18-fluoro-2-deoxyglucose, to preferentially label
82 tumors for cancer imaging (PET-scans) [6]. So far, trials using 2DG as the sole chemotherapeutic agent have
83 failed because of the relative toxicity of this molecule, however strategies using 2DG or other 2-deoxy-
84 substituted versions of glucose in combination with other drugs are under study and are promising [6].

85 2DG has also been extensively used to understand glucose signaling in micro-organisms such as the
86 baker's yeast *Saccharomyces cerevisiae*, where it has been instrumental to delineate the molecular
87 mechanisms by which glucose regulates gene expression [reviewed in 3]. The metabolism of *S. cerevisiae* is
88 biased towards the preferential use of glucose as a carbon source. At the molecular level, glucose represses
89 the expression of many genes involved in respiratory metabolism or in the use of other carbon sources,
90 thereby favoring the preferential use of glucose by fermentation [7]. Among the actors in charge of adapting
91 the transcriptional program with respect to glucose availability is the yeast orthologue of AMPK, Snf1 [7, 8].
92 Snf1 is the catalytic subunit of a heterotrimeric complex which is active in the absence of glucose in the
93 medium. A canonical example of a Snf1-regulated transcription is that of the invertase *SUC2*, required for
94 sucrose hydrolysis and metabolism. Transferring yeast cells to sucrose medium activates Snf1, causing the
95 phosphorylation of the transcriptional repressor Mig1, its translocation out of the nucleus and the
96 derepression of *SUC2* [9, 10].

97 Snf1, like other kinases of the AMPK family, is activated by phosphorylation of a residue in its activation
98 loop [11]. This involves one of 3 upstream kinases whose activity is, surprisingly, not regulated by glucose.

99 Rather, evidence suggests that Snf1 activity is regulated by its dephosphorylation by the Protein Phosphatase
100 1 (PP1) complex made of the catalytic subunit, Glc7, and the glucose-specific regulatory subunit Reg1 [12].
101 How PP1 activity is linked to glucose availability is not yet clear, but deletion of *REG1* leads to constitutive
102 Snf1 activity and to the expression of glucose-repressed genes even in the presence of glucose [13].
103 Another phenotype displayed by the *reg1Δ* strain is its ability to grow robustly in presence of 2DG [3, 14,
104 15]. This is attributed to the constitutive activation of Snf1 in this mutant, as mutations in *SNF1* cause
105 hypersensitivity to 2DG and yeast lacking both Reg1 and Snf1 are also hypersensitive [16].
106 Despite the multifaceted cellular effects of 2DG, cells can indeed overcome 2DG toxicity by mechanisms
107 that are currently being unraveled [reviewed in 3, 15]. A prolonged exposure of HeLa cells in 2DG-containing
108 medium gave rise to resistant clones [17]. These cells displayed a high phosphatase activity towards 2DG-6-
109 phosphate (2DG-6-P), suggesting the presence of an enzyme that could detoxify this metabolite back into
110 2DG and thus prevent the metabolic blockade. Studies in yeast also identified phosphatases, named Dog1
111 and Dog2, with a similar activity *in vitro* and whose overexpression allows growth in 2DG-containing medium
112 [18, 19]. Recently, we found that the most abundant isoform, Dog2, is itself a glucose-repressed gene and
113 thus is regulated by Snf1/AMPK function [20]. This partially explains why strains with high Snf1/AMPK activity
114 are resistant to 2DG, such as *reg1Δ* [14, 16], other *reg1* mutant alleles [20, 21], a viable *glc7* mutation (Q48K)
115 [21] or gain-of-function mutations in components of the AMPK complex [16, 21, 22]. However, additional
116 resistance mechanisms independent of *DOG2* expression are at stake in these strains [20, 21]. This is
117 suggested by the observation that *DOG2* deletion does not completely re-sensitize *reg1*Δ mutants to 2DG,
118 and a point mutation in *REG1* (*reg1-P231L*) confers 2DG resistance but does not impact on the glucose-
119 mediated repression of genes [21]. Thus, Snf1 likely controls additional factors participating in 2DG
120 resistance.
121 One such candidate is the arrestin-related protein, Rod1. Arrestin-related proteins (ARTs) are important
122 regulators of plasma membrane protein endocytosis in response to extracellular cues [23, 24]. ARTs recruit
123 the ubiquitin ligase Rsp5 to nutrient transporters at the plasma membrane, promoting their subsequent
124 ubiquitylation and endocytosis [25]. ART activity is regulated by nutrient signaling pathways, allowing to
125 remodel the landscape of transporters at the plasma membrane to meet the physiological needs of cells
126 facing a nutrient challenge [26, 27]. Particularly, Rod1 regulates endocytosis in response to glucose
127 availability, and its activity is oppositely regulated by Snf1 and PP1 [28-30], being a direct target of Snf1 [31].
128 A genome-wide screen revealed that *rod1Δ* is indeed resistant to 2DG [14], thus the Snf1-mediated inhibition
129 of Rod1 might contribute to 2DG resistance.

130 Point mutations aimed at abolishing Rod1 interaction with the ubiquitin ligase Rsp5, thereby annihilating
131 their function as adaptor proteins in endocytosis, increased resistance to 2DG suggesting that it mediates
132 2DG toxicity through its function in endocytosis [32]. 2DG resistance of the *rod1Δ* strain is further increased
133 by the additional deletion of the *ROD1* paralogue *ROG3* [32]. Rod1 (and Rog3, to a lesser extent) controls the
134 endocytosis of the glucose transporters Hxt1 and Hxt3 triggered in response to 2DG exposure, and
135 overexpression of the same transporters in a *snf1Δ* mutant restored partial resistance to 2DG [32]. Deletion
136 of *ROD1* and *ROG3* stabilized hexose transporters at the plasma membrane in *snf1Δ* and restored its 2DG-
137 sensitivity to WT levels [32]. However, whether the effects of 2DG on endocytosis extend beyond glucose
138 transporters is unknown, and there is currently no molecular understanding of how transporter
139 stability/localization contributes to 2DG resistance.
140 In this study, we examined the effects of 2DG on endocytosis and found that 2DG triggers the endocytosis
141 of many plasma membrane proteins, most of which depend on Rod1. Mechanistically, we show that opposite
142 to the situation in mammalian cells, 2DG treatment leads to the dephosphorylation of Snf1/AMPK and
143 several targets including Rod1 in a-PP1 dependent manner. This favors Rod1 function and thus provides a
144 rationale as to why this arrestin is central to 2DG-induced endocytosis. Finally, we demonstrate that 2DG
145 resistance of the *rod1Δ* strain relies on the maintenance of active glucose transporters at the membrane,
146 where they can increase glucose uptake and contribute to detoxifying 2DG out of the cells, thus terminating
147 the detoxification process.
148

149 # Results

150 **2DG triggers the endocytosis of many plasma membrane proteins**

151 We previously described the proteomic changes occurring in response to 2DG and focused on proteins
152 upregulated in this condition [20]. In addition, a few transmembrane proteins of the plasma membrane
153 displayed a significantly decreased abundance after 2h30 2DG treatment, including the amino acid permease
154 Tat1 and the hexose transporter Hxt2 [20]. This could either be caused by a decreased synthesis or an active
155 degradation by endocytosis. We verified this by looking at the regulation of the endogenously GFP-tagged
156 proteins. Treatment of glucose-grown cells with 0.2% 2DG led to the targeting of plasma membrane-localized
157 Tat1 and Hxt2 (**Fig 1A**) to the vacuole, which was accompanied by their degradation (**Fig 1B**). Of note, we
158 observed that the vacuole was strongly fragmented in response to 2DG (**Fig S1**), confirming recent findings
159 [33]. This may be due to the fact that 2DG causes ER stress in yeast [20], which itself induces vacuolar
160 fragmentation [34].

161 Tat2 and Hxt2 endocytosis in response to 2DG is reminiscent of the behavior of the low affinity hexose
162 transporters Hxt1 and Hxt3 [32]. To document the extent of plasma membrane remodeling caused by 2DG
163 exposure, we studied the regulation of a representative subset of plasma membrane proteins tagged with
164 GFP at their endogenous loci before and after 2DG treatment. This included transporters of various
165 substrates or structural classes, as well as receptor/sensor proteins whose expression could be detected in
166 glucose-grown cells. This showed that many of these membrane proteins are endocytosed in response to
167 2DG (**Fig 1D, Fig S2**).

168 In yeast, nutrient transporter endocytosis is driven by their ubiquitylation at the plasma membrane,
169 which relies on the action of the ubiquitin ligase Rsp5 and adaptor proteins of the arrestin-like family (ARTs)
170 [24, 27]. Previous work highlighted the importance of the arrestin-related protein Rod1 in the 2DG-induced
171 endocytosis of Hxt1 and Hxt3 [32]. Indeed, we found that most of the cargoes studied here depended on
172 Rod1 for their 2DG-induced endocytosis (**Fig 1D, Fig S2**). Although the Rod1 paralogue Rog3 displays some
173 level of functional redundancy with Rod1 [32], Rog3 was not responsible for the endocytosis of the Rod1-
174 independent cargo Lyp1 (**Fig S3**), although this may be the case for other cargoes. Altogether, these results
175 indicate a prominent role for the ART protein Rod1 in 2DG-induced endocytosis.

176

177 **2DG triggers endocytosis by inducing Rod1 dephosphorylation and ubiquitylation**

178 We then focused on understanding why Rod1 function is so central for 2-deoxyglucose endocytosis. In
179 the case of glucose-induced endocytosis, Rod1 activity is regulated through changes in its post-translational
180 modifications [28, 29]. In a glucose-deprived medium, AMPK/Snf1 is active and phosphorylates Rod1,

181 inhibiting its function [28, 29, 31, 35]. Conversely, glucose addition in the medium leads to Rod1
182 dephosphorylation in a PP1-dependent manner, followed by its ubiquitylation by Rsp5 [28, 29]. These
183 modifications promote its activity as an Rsp5 adaptor, leading to transporter ubiquitylation, endocytosis and
184 vacuolar sorting [28, 29, 35]. Similarly, 2DG addition to glucose-grown cells triggers Rod1 ubiquitylation in an
185 Rsp5- and PP1-dependent manner, but paradoxically 2DG was also reported to increase Snf1 activity [30, 32].
186 Thus, how 2DG regulates the relative activities of Snf1/PP1 and how this impacts on Rod1 activity are not
187 fully understood.

188 Previously, the effect of 2DG on Rod1 post-translational modifications was evaluated using an 3HA-
189 tagged construct [32]. Although Rod1-3HA could support the glucose-induced endocytosis of Jen1 [28], we
190 realized that it was unable to restore the 2DG-induced endocytosis of Hxt1-GFP and Hxt3-GFP in a *rod1Δ*
191 context , contrary to Flag-tagged Rod1 (Flag) which functionally behaved like the wild-type protein (**Fig S4A**
192 and **B**). We then re-evaluated Rod1 post-translational modifications using this functional construct. As for
193 Rod1-3HA [32], we observed drastic changes in Rod1 mobility on gel after 2DG treatment (**Fig 2A**). In
194 glucose-grown cells, Rod1-Flag migrated as a diffuse band resulting from a mild phosphorylation, as
195 determined by phosphatase treatment, and similarly to previously published results using Rod1-3HA [28, 32]
196 (**Fig 2A**). This pattern gave rise to two discrete bands upon 2DG exposure, with the upper band
197 corresponding to ubiquitylated Rod1, as shown by its disappearance when mutating the known ubiquitylated
198 lysine(s) (K235, K245, K264, K267) on Rod1 as described previously [28, 32]. The lower band corresponded to
199 a dephosphorylated species of Rod1, as demonstrated by the fact that it migrated similarly as Rod1-Flag from
200 phosphatase-treated extracts (**Fig 2B**). This fits with previous results obtained in the context of glucose-
201 induced endocytosis, in which Rod1 ubiquitylation was preceded by its dephosphorylation [28, 29]. As
202 expected, Rod1 was constitutively phosphorylated in the PP1 phosphatase mutant *reg1Δ* and this
203 phosphorylation was no longer affected by 2DG treatment (**Fig 2B**). In contrast, mutations in the described
204 Rod1 phosphatase, calcineurin (*cnb1*Δ) [36, 37] or in various signaling pathways whose activation is triggered
205 by 2DG treatment [20] (MAPK= *slt2*Δ, *hog1*Δ; UPR: *hac1*Δ) had no impact (**Fig 2C**). This suggested that PP1
206 activity is required for the 2DG-induced dephosphorylation of Rod1. Moreover, deletion of *SNF1* or mutation
207 of 12 serine residues within potential Snf1 consensus sequences (see Material and Methods) [36] led to a
208 profile comparable to that obtained in 2DG-treated cells, suggesting that lack of Rod1 phosphorylation
209 mimics 2DG-treatment (**Fig 2D**).

210 Having confirmed how Rod1-Flag is post-translationally modified in response to 2DG, we assessed the
211 functional consequences abrogating these modifications on the function of Rod1 in endocytosis. Instead of
212 focusing on Hxt1 or Hxt3, which are glucose-regulated [32], we used Ina1-GFP as a model cargo (see **Fig 1D**

213 and Fig S5). Ina1 is a protein of the SUR7/Pall family, with carries 3 predicted transmembrane domains and
214 localizes to the plasma membrane [38]. Mutation of the ubiquitylation site(s) within Rod1 resulted in a
215 slowdown of Ina1 endocytosis, whereas mutation of the PPxY motifs preventing the interaction with Rsp5
216 [28] completely abolished it (Fig 2E). This was confirmed by data obtained on the endocytosis of Hxt1-GFP
217 and Hxt3-GFP (Fig S6). Growth assays demonstrate that Rod1 activity in endocytosis correlated with 2DG
218 sensitivity (Fig 2F). Interestingly, despite the fact that Rod1-S12A-Flag appeared constitutively
219 dephosphorylated/ubiquitylated (see Fig 2D), Ina1-GFP endocytosis still relied on 2DG addition, suggesting
220 yet another layer of regulation. Accordingly, Ina1 endocytosis was still regulated by 2DG in the *snf1Δ* mutant
221 (Fig 2G), and so were other Rod1 cargoes (Fig S7). Thus, Rod1 dephosphorylation (or lack of phosphorylation)
222 is not sufficient to trigger endocytosis, suggesting yet an additional level of regulation.
223
224 **2DG promotes the PP1-dependent dephosphorylation of Snf1 and several of its targets**
225 The fact that 2DG triggers a PP1-dependent dephosphorylation of Rod1 contrasted with previous results
226 showing that 2DG induces a mild phosphorylation (activation) of the PP1 substrate Snf1 within 2h of
227 treatment [16], similar to observations in mammalian cells [3, 39]. To explain this discrepancy, we
228 reexamined the effects of 2DG on Snf1 signaling. For this, we followed Snf1 phosphorylation after 2DG
229 treatment using antibodies directed against the activated (phosphorylated) form of human AMPKα, which
230 cross-reacts with yeast Snf1 [40]. As a control for total Snf1, anti-polyhistidine antibodies can be used
231 because Snf1 contains a stretch of 13 histidine residues that can be used for its detection [40]. However, the
232 signals were sometimes very weak and so we completed our results with an endogenously GFP-tagged
233 version of Snf1. We found this version to be fully functional (Fig S8), as follows. Briefly, (i) the Snf1-GFP strain
234 was able to use sucrose as a C source (Fig S8A), (ii) Mig1-Flag phosphorylation was similar in the Snf1-GFP
235 strain as it was in the WT upon varying glucose concentrations, (iii) Snf1-GFP phosphorylation increased at
236 low glucose concentrations, which was counteracted by glucose addition, and finally (iv) Snf1-GFP
237 phosphorylation increased in the *reg1Δ* mutant (Fig S8B). These data validate Snf1-GFP as a suitable epitope-
238 tagged version of Snf1.
239 After 10 min 2DG treatment, we never observed Snf1 activation, even at higher 2DG concentration (Fig
240 3A). On the contrary, 2DG consistently decreased Snf1 phosphorylation within minutes after treatment (Fig
241 3B-C). A kinetic analysis of phospho-Snf1 response to 2DG confirmed a drop in Snf1 phosphorylation that was
242 followed by an increase at later time points (Fig 3C). Snf1 dephosphorylation by 2DG required the PP1
243 subunit Reg1, thus mimicking the effect that glucose has on glucose-starved cells. Similar observations were
244 made for the Snf1 substrate Rod1-Flag (Fig 3C). Altogether, we conclude that 2DG triggers an immediate and

245 transient PP1-dependent dephosphorylation of Snf1, consistent with our (Fig 2) and others' [32] observations
246 on Rod1.
247 This was further confirmed by studying another Snf1 substrate, the transcriptional repressor Mig1 [41,
248 42] which was also dephosphorylated after 2DG treatment in a PP1-dependent manner (Fig 3D). Again, this
249 mimicked the situation described when glucose-starved cells are treated with glucose [43]. Thus, 2DG
250 triggers both an immediate and transitory PP1-dependent inhibition of Snf1, and the dephosphorylation of
251 Snf1 substrates such as Mig1 or Rod1.
252
253 **Snf1 inactivation by 2DG requires 2DG phosphorylation by Hxk2**
254 We then investigated the origin of the signal triggering the PP1-dependent dephosphorylation of
255 substrates. 2DG is taken up by hexose transporters and is then phosphorylated into 2DG6P [44], which
256 interferes with several metabolic pathways. Hxk2 is the main hexokinase isoform expressed in glucose-grown
257 yeast cells [45] and we studied its contribution in 2DG phosphorylation by measuring 2DG6P appearance
258 after 2DG treatment using an enzyme-based assay [46]. After 15 min exposure to 0.2% 2DG, 2DG6P was
259 readily detectable in WT cells (Fig 4A). In *hxk2Δ*, 2DG6P only reached 25% of the WT value (Fig 4A),
260 suggesting that Hxk2 is the main 2DG-phosphorylating enzyme.
261 2DG phosphorylation by hexokinase into the dead-end metabolite 2DG6P requires ATP and causes a
262 strong ATP depletion [47, 48]. This can be visualized within minutes after 2DG addition in WT cells using an
263 optimized, pH-insensitive version of the AT1.03 ATP FRET biosensor [49] (Fig 4B). The decrease in FRET signal
264 occurred only upon 2DG treatment and revealed changes in ATP content as demonstrated using a mutant
265 version of the FRET sensor which does not bind ATP [49] (Fig 4B). We found that comparatively to the WT,
266 the drop in FRET was lower in *hxk2Δ* cells, again suggesting that Hxk2 is key for 2DG phosphorylation (Fig 4C).
267 In line with these findings, we found that neither Snf1 nor Rod1 were dephosphorylated in response to
268 2DG in the *hxk2Δ* mutant (Fig 4D). Similarly, 2DG no longer triggered Ina1-GFP endocytosis in this strain (Fig
269 4E), nor that of Hxt1 and Hxt3 (Fig S9A). Overall, our data suggest that either Hxk2 itself or 2DG
270 phosphorylation is required for the 2DG-mediated activation of PP1. Noteworthy, overexpression of the
271 2DG6P phosphatase Dog2, but not that of its catalytic-dead mutant (Dog2-DDAA), also abolished Ina1-GFP
272 endocytosis (Fig 4F) and that of Hxt1 and Hxt3 (Fig S9B), suggesting that 2DG-6-P levels directly or indirectly
273 control PP1 activity. Altogether, we propose that 2DG phosphorylation by Hxk2 triggers a PP1-dependent
274 Snf1 dephosphorylation, Rod1 dephosphorylation and endocytosis.
275

276 **Stabilization of glucose transporters at the plasma membrane confers 2DG resistance to the *rod1Δ***
277 **mutant**

278 So far, our data provide mechanistic insights as to how 2DG triggers endocytosis through AMPK
279 inhibition and Rod1 activation. *ROD1* deletion leads to 2DG resistance [14], but the underlying mechanism
280 remains unclear. We previously described that a frequent strategy leading to 2DG resistance involves an
281 increased expression of the Dog2 phosphatase at the transcriptional level [20]. However, using a *pDOG2*:LacZ
282 reporter, we found that this was not the case in the *rod1*Δ mutant, suggesting a distinct mechanism (Fig 5A).

283 The 2DG resistance of the *rod1Δ* strain is exacerbated upon the further deletion of its paralogue *ROG3*
284 [32], and other data indicate that 2DG resistance correlates with Rod1 activity in endocytosis [32] (see also
285 Fig 2F). Since Rod1 has a central role in plasma membrane protein remodeling by 2DG (Fig 1D and Fig S2), we
286 first hypothesized that the 2DG-mediated activation of Rod1 might trigger excessive endocytosis that would
287 be deleterious for the cell, and could be counteracted by *ROD1* deletion. We postulated that 2DG resistance
288 originates from the stabilization of one or several Rod1-regulated cargoes at the plasma membrane. We
289 initially focused on the low affinity hexose transporters, Hxt1 and Hxt3, for the following reasons. First, the
290 hypersensitivity of the *snf1Δ* mutant to 2DG is rescued by overexpression of Hxt1 and Hxt3 through an
291 unknown mechanism [32]. Second, duplication of a chromosomal region containing hexose transporter
292 genes (*HXT3*, *HXT6* and *HXT7*) confers 2DG-resistance in a dominant manner [22]. Since these transporters
293 are not endocytosed in the *rod1Δ* mutant (Fig 1C and S2) [32], we thus considered that their stabilization
294 could contribute to 2DG resistance. Indeed, deletion of either *HXT3* or *HXT1* abolished the 2DG resistance of
295 the *rod1Δ* mutant strain (Fig 5B), showing that both transporters are required for this process. In contrast,
296 deletion of the high-affinity hexose transporter gene *HXT6* did not cause the same phenotype (Fig 5B).
297 Although, it seems that only low-affinity hexose transporters promote 2DG resistance, this conclusion may
298 be biased by the fact that low- and high-affinity hexose transporters are expressed to a lower level, the
299 former contributing more to glucose uptake than the latter in glucose-rich conditions [50].

300 The growth defect of the obtained *rod1Δ hxt3Δ* strain on 2DG was restored by expressing a GFP-tagged
301 version of Hxt3 driven by its own promoter on a low-copy (centromeric) plasmid (Fig 5C). This mild
302 overexpression of Hxt3 also further increased 2DG resistance of the already resistant *rod1Δ* strain but had no
303 effect on WT cells. Only a stronger expression of Hxt3 from a multicopy (2µ) plasmid conferred resistance to
304 WT cells (Fig 5D), whereas that of Hxt1 had little or no effect as found previously [32]. Hxt1 and Hxt3 may
305 have different functions regarding 2DG resistance, since Hxt1 overexpression did not compensate for the loss
306 of Hxt3 in the *rod1Δ hxt3Δ* background (Fig 5D). Overall, we conclude that a high expression of glucose
307 transporters generally correlates with 2DG resistance.

308 Structure/function studies of transporters [reviewed in 51] identified residues critical for hexose binding
309 and translocation. In particular, residue N317 of the human glucose transporter GLUT1 binds glucose [52, 53]
310 and mutation of the corresponding residue in yeast transporters alters substrate specificity and transport
311 [54-56]. Particularly, mutation of this residue in Hxt1 (N370A) [57] and other yeast hexose transporters [54,
312 58] abolished glucose uptake. We mutated the corresponding residue in Hxt3 (N367A) and found that its
313 overexpression no longer rescued growth on 2DG, further linking glucose transporter function with 2DG
314 resistance (Fig 5C).
315
316 **Stabilization of glucose transporters at the plasma membrane facilitates glucose uptake and 2DG**
317 **export**
318 The fact that glucose transport correlates with 2DG resistance was counterintuitive because 2DG enters
319 into cells through glucose transporters [44], thus their stabilization at the cell surface may increase 2DG
320 uptake. Indeed, deleting both *HXT1* and *HXT3* causes partial resistance to 2DG (Fig 6A), indicating that 2DG is
321 mostly transported into cells through these transporters.
322 We considered two hypotheses to explain how glucose transporter accumulation at the plasma
323 membrane results in 2DG resistance. First, by depleting glucose transporters from the plasma membrane,
324 2DG-induced endocytosis could lower glucose intake at a time where glycolysis is already impacted, resulting
325 in energy shortage as previously proposed [32]. Preventing endocytosis may therefore attenuate the
326 glycolysis blockade by maintaining glucose uptake. Alternatively, transporters present at the cell surface may
327 instead favor 2DG detoxification and release into the medium, as previously observed [44] since the
328 directionality of transport (import or export) through hexose transporters is dictated by the concentration
329 gradient.
330 We first tested whether *rod1Δ* cells could detoxify 2DG6P more efficiently than WT cells. Cells were
331 treated for 2h with 2DG, and 2DG6P was generated at comparable levels in both strains (Fig 6B).
332 Interestingly, in WT cells, the concentration of 2DG6P after 2h 2DG treatment was comparable to that
333 observed after 15 min (Fig 6C), showing that saturation is reached very early after treatment. Cells were then
334 transferred to a 2DG-free medium for 30 min and 2DG6P was assayed again. In both strains, 2DG6P
335 concentration decreased during these 30 min, revealing they could detoxify 2DG6P (Fig 6B). However, the
336 2DG6P content was much lower in *rod1Δ* than in WT cells, suggesting that 2DG6P is better detoxified in this
337 strain. Therefore, the endocytosis blockade caused by the deletion of *ROD1* allows a better detoxification of
338 2DG. To address whether this involved Hxt3, we repeated this experiment in a *rod1Δ hxt3Δ* context (Fig 6D).
339 We found that this restored 2DG6P content to comparable levels as those of the WT strain, whereas the

340 deletion of *HXT3* alone had no significant effect on 2DG6P accumulation or disappearance. Therefore, Hxt3 is
341 required for the increased detoxification of 2DG6P observed in the *rod1Δ* cells.
342 We also tested whether hexose transporters maintenance at the membrane impacts on glucose uptake,
343 by using an intracellular glucose FRET sensor based on the bacterial glucose/galactose-binding transport
344 protein MglB [59]. Previous work established that 2DG does not bind significantly to this probe, allowing its
345 use to measure glucose content in our setting [60]. We assessed intracellular glucose following glucose
346 exposure after a 4h-treatment with 2DG, and found that glucose accumulated slightly more in *rod1Δ* than in
347 WT cells (**Fig 6E-F**). This depended on the presence of the glucose transporter Hxt3, since the additional
348 deletion of *HXT3* in the context of *rod1Δ* restored glucose uptake to WT levels (**Fig 6E-F**) and 2DG sensitivity
349 (**Fig 5B-D**). Finally, deletion of both *HXT1* and *HXT3* strongly impaired glucose uptake, as expected. Thus,
350 *ROD1* deletion could facilitate cell survival independently of 2DG detoxification by allowing a sustained
351 glucose uptake. This was further illustrated by the fact that deletion of *ROD1* conferred 2DG resistance to a
352 strain lacking both *DOG1* and *DOG2*, that are central to 2DG detoxification (**Fig 6G**). Therefore, the lack of
353 endocytosis of hexose transporters protects cells from 2DG toxicity by several mechanisms.
354

355 ## Discussion

356

357 Several strategies are known to modulate 2DG sensitivity/resistance in yeast [3]. The most common
358 mechanism is through the aberrant activation of the AMPK orthologue, Snf1, either by gain-of-function
359 mutation in constituents of the AMPK heterotrimeric complex, or by loss-of-function mutations of its
360 inhibitory phosphatase (PP1: Glc7/Reg1) [3, 21]. How AMPK hyperactivation contributes to 2DG resistance is
361 not fully understood, but we previously found that this partially occurs through the expression of the
362 detoxification enzyme Dog2 [20]. Here, we provide important insights into the cellular effects that 2DG has
363 on AMPK signaling, how this impacts Rod1 activity and subsequently, on endocytosis, and how endocytosis
364 interference leads to 2DG resistance through the control of glucose transport activity.

365 We first report that 2DG acts as a strong endocytosis signal, leading to the endocytosis of many plasma
366 membrane proteins. These include a GPCR (Ste2), various classes of transporters, such as permeases, solute
367 carriers such as multidrug transporters of the major facilitator superfamily (MFS) or ATP-binding cassette
368 (ABC) types. This massive 2DG-induced endocytosis of membrane proteins is reminiscent of that observed in
369 other situations of metabolic stresses such as acute glucose or nitrogen starvation [61-63], or upon
370 treatment with other drugs, stressors or heat shock [26, 64-69]. Because 2DG is an artificial molecule, the
371 observed endocytosis is unlikely to originate from an adaptation strategy but rather informs us that 2DG-
372 induced metabolic blockade triggers endocytosis through mechanisms that we further explored.

373 First, our work highlights the major role played by the arrestin Rod1 in 2DG-induced endocytosis. Rod1
374 participates in the endocytosis of the glucose transporters Hxt1 and Hxt3 upon 2DG treatment [32], and we
375 extend these findings to many other membrane proteins. Using a tagged but fully functional protein, we
376 confirm previous findings [32] that 2DG treatment strongly affects Rod1 post-translational modifications
377 (phosphorylation and ubiquitylation), reminiscent of past studies focusing on the regulation of Rod1 by
378 glucose availability [28, 29, 31, 36]. Phosphorylation is a frequent mechanism for arrestin inhibition [28, 65,
379 70, 71], perhaps by introducing negative charges that may hinder transporter interactions [63] [reviewed in
380 27]. Accordingly, Rod1 dephosphorylation and its subsequent ubiquitylation are required for its activity in
381 endocytosis [28, 29]. Arrestin ubiquitylation is often required for their function [28, 70, 72], and this may
382 favor interaction with Rsp5 and thus the Rsp5-mediated ubiquitylation of transporters [73]. Overall, we
383 propose that 2DG induces an aberrant activation of Rod1 which explains the increased endocytosis observed
384 in response to 2DG.

385 Second, we gained insights into how 2DG triggers these changes on Rod1, given that the precise effect
386 of 2DG on Rod1 regulatory kinase(s) or phosphatase(s) was unclear until now. 2DG is well known to trigger

387 AMPK activation in mammalian cells even at short timepoints [3, 39, 74], and a similar but milder effect was
388 reported for Snf1 in yeast after 2h treatment [16]. Yet, this apparent activation of Snf1 did not translate into
389 an increased phosphorylation of its substrate Mig1 [16], and the reported dephosphorylation of Rod1 in
390 these conditions was also not in line with an increased Snf1 activity. Rather, by focusing on shorter
391 timepoints, we observed a sharp decrease in Snf1 phosphorylation shortly after 2DG addition. Thus, 2DG
392 treatment rapidly inhibits yeast Snf1 activity, contrary to observations on mammalian AMPK. We also found
393 that after this initial drop in phosphorylation, Snf1 activity slowly increases over time to reach back its initial
394 activity, or even higher levels [16]. However, we expect that hours of 2DG treatment strongly perturb cellular
395 physiology and it may be delicate to specifically pinpoint the mechanisms leading to Snf1 activation in this
396 context.

397 Beyond the fact that it involves PP1, the mechanism by which Snf1 dephosphorylation is stimulated by
398 2DG shortly after treatment remains to be established. However, several possibilities can be considered.
399 First, through a derived metabolite or a metabolic imbalance caused by the glycolytic inhibition, 2DG could
400 activate the Glc7/Reg1 PP1 subcomplex, for example by favoring its assembly or its recruitment onto
401 substrates. A second and more likely possibility is derived from previous work on Snf1 dephosphorylation in
402 response to glucose. Using analog-sensitive alleles of a Snf1-activating kinase or of Snf1 itself, it was shown
403 that PP1 activity towards Snf1 is stimulated by glucose whereas PP1 activity towards Mig1 remains constant
404 regardless of the glucose status [12]. Whether this is due to a better accessibility of Snf1, an increased
405 recruitment of PP1, or a stimulation of PP1 activity, the same mechanism could be at stake in response to
406 2DG. The maintenance of PP1 activity towards Snf1 substrates (eg. Mig1) in a context where Snf1 is
407 inactivated would be sufficient to explain why phosphorylation of Mig1 decreased in response to 2DG within
408 a few minutes. This may also explain observations on Rod1 which also requires PP1 for its dephosphorylation
409 in response to glucose [28, 29] or 2DG [this study and 32]. The increased dephosphorylation of Snf1 in
410 response to 2DG is reminiscent to that observed when glucose is added to cells deprived of glucose [75].
411 Thus, shortly after treatment and even in glucose-grown cells, 2DG treatment mimics glucose-replete
412 conditions rather than starvation, and part of the early 2DG response involves a drop in Snf1 activity.

413 This inactivation of Snf1 by 2DG involves Hxk2, as 2DG was no longer able to trigger Snf1/Rod1
414 dephosphorylation or the endocytosis of Ina1, Hxt1 and Hxt3 in the *hxk2Δ* strain. Hxk2 may either have a
415 unique function in 2DG toxicity beyond its enzymatic function, but we favor the hypothesis that Hxk2
416 mediates 2DG-induced signaling through its unique ability to generate 2DG6P. Despite the fact that 2DG6P
417 can be generated by other sugar-phosphorylating enzymes (Hxk1 and glucokinase Glk1) *in vitro* [21], only
418 *HXK2* deletion causes 2DG resistance [14, 16, 20, 21]. Moreover, our *in vivo* data suggest that Hxk2 is the

419 most prominent 2DG-phosphorylating enzyme, since *hxk2Δ* cells have a lower 2DG6P content and 2DG has a
420 lower impact on the ATP status in these cells. The lack of effect of Hxk1 or Glk1 on 2DG toxicity could be
421 explained by a lower expression level or other *in vivo* regulatory mechanisms that would prevent an efficient
422 2DG phosphorylation. Interestingly, both *HXK2* deletion and overexpression of the 2DG-6-P phosphatase
423 Dog2, which converts 2DG-6-P back into 2DG, protect *snf1Δ* against 2DG hypersensitivity [16, 20], so both
424 may act through a decreased 2DG6P content. More generally, 2DG has virtually no effect in strains
425 overexpressing Dog2, further suggesting that 2DG6P (or a derived metabolite) contributes to the
426 dephosphorylation of Snf1 and its substrates. Further work should be aimed at understanding how the
427 PP1/Snf1 balance is controlled by 2DG at the molecular level, which may help decipher the long-sought
428 mechanism by which glucose-starved cells react to glucose addition [12, 75-77].

429 After delving into the mechanisms by which 2DG triggers endocytosis through the modulation of glucose
430 signaling pathways and Rod1 activity, we also obtained insights into how *ROD1* deletion results in 2DG
431 resistance. The study of Rod1 point mutants indicate a correlation between endocytosis and 2DG resistance
432 [this work, and 32] and Hxt1 and Hxt3 stabilization at the plasma membrane was necessary for 2DG
433 resistance, in line with the fact that their overexpression allows 2DG resistance [32]. Although Hxt1 and Hxt3
434 are the main transporters involved in 2DG uptake, their maintenance at the plasma membrane is required
435 for long-term resistance through two possible pathways that possibly synergize (**Fig 7**). The first pathway
436 involves 2DG detoxification. Indeed, 2DG triggers the induction of the Dog1 and Dog2 phosphatases which
437 dephosphorylate 2DG6P into 2DG [20], the latter of which could presumably be exported once its cytosolic
438 concentration is higher than that of the medium and provided that hexose transporters be present at the
439 plasma membrane. This is in line with observations showing that (i) transport across the membrane is
440 required to confer resistance, (ii) the same transport systems are used both for 2DG and glucose [44], and
441 (iii) proteins of the GLUT/HXT family support bidirectional fluxes across the membrane [eg. GLUT2 in
442 hepatocytes, reviewed in 78]. Accordingly, we found that *ROD1* deletion increases the ability to detoxify
443 2DG6P, and this depended on the presence of Hxt3 . Thus, stabilizing glucose transporters at the plasma
444 membrane might allow the release of 2DG back to the medium, but this possibility should be further
445 explored in the future. The second pathway posits that transporter stabilization at the plasma membrane
446 allows a sustained glucose import, and thus may help bypass the 2DG-induced glycolytic blockade. Over time,
447 2DG6P synthesis and accumulation should inhibit hexokinase and thus blocks glucose phosphorylation, which
448 itself drives glucose import [79] [reviewed in 80], but given the existence of detoxification mechanisms, the
449 glycolytic blockade may be only temporary. Increasing transporter availability should in principle boost

450 glucose import and help glycolysis recover, and accordingly, *rod1Δ* cells contain more glucose than WT cells
451 when exposed to glucose after 2DG treatment.
452 In mammalian cells, 2DG causes a fast energy depletion and AMPK activation [39]. This is exemplified by
453 the opposite effect that 2DG has on the endocytosis of glucose transporters. In hepatocytes, the 2DG-
454 induced activation of AMPK triggers the phosphorylation of the arrestin-like protein TXNIP, resulting in its
455 degradation and stabilization of the glucose transporter GLUT1 [74], a response which is consistent with
456 energy depletion and starvation response. In contrast, 2DG transiently inhibits yeast Snf1, thus promoting
457 Rod1-mediated glucose transporter endocytosis [this work and 32]. This somewhat paradoxical response
458 likely reveals that in yeast, 2DG causes energy deprivation but is also likely sensed as excess glucose (causing
459 a decreased Snf1/AMPK activity). The differences in 2DG signaling between these two model systems may
460 originate from evolutionary differences regarding their ability to detect glucose as a signaling molecule, in
461 addition to being a source of energy. Glucose is the preferred carbon source for *Saccharomyces cerevisiae*
462 and is mostly used by fermentation, implying a high glycolytic flux to sustain proliferation. Yeast has evolved
463 various sensing systems at the plasma membrane to detect extracellular glucose, that are wired into various
464 signaling pathways [81]. It is likely that Hxk2 and/or glucose phosphorylation itself acts as a glucose sensor
465 within the Snf1/AMPK pathway [82-84], and 2DG phosphorylation by Hxk2 may produce a glucose-replete
466 signal, leading to Snf1 inactivation despite changes in the energy load. This is probably only true shortly after
467 2DG treatment, before 2DG inhibits other aspects of cellular physiology (such as protein glycosylation or
468 structural sugar metabolism) leading to a complex response through stress-signaling pathway (such as UPR
469 or MAPK-based signaling) [3, 20]. In conclusion, the characterization of 2DG resistance strategies led once
470 more to a better understanding of the cellular effects of 2DG and the diversity of mechanisms that can be
471 deployed to bypass 2DG-induced metabolic inhibition.
472

473 # Materials and Methods

474 **Yeast strain construction and growth conditions**

475 All yeast strains used in this study derive from the *Saccharomyces cerevisiae* BY4741 or BY4742 background
476 and are listed in table S1. Apart from the mutant strains obtained from the yeast deletion collection
477 (Euroscarf) and the fluorescent GFP-tagged strains originating from the yeast GFP clone collection {Huh, 2003
478 #123}, all yeast strains were constructed by transformation with the standard lithium acetate–polyethylene
479 glycol protocol using homologous recombination and verified by polymerase chain reaction (PCR) on
480 genomic DNA prepared with a lithium acetate (200 mM)/SDS (0.1%) method (104). Yeast cells were grown in
481 YPD medium (2%) or in SC medium [containing yeast nitrogen base (1.7 g/liter; MP Biomedicals), ammonium
482 sulfate (5 g/liter; Sigma-Aldrich), the appropriate drop-out amino acid preparations (MP Biomedicals), and
483 2% (w/v) glucose, unless otherwise indicated]. Precultures were incubated at 30°C for 8 hours and diluted in
484 the evening to 20-ml cultures to reach mid-log phase the next morning. 2DG (Sigma) was added to mid-log
485 phase yeast cultures grown overnight to final concentrations of 0.2% (w/v) and incubated for the indicated
486 times.
487

488 **Plasmid construction**

489 All plasmids used in this study are listed in table S2.
490 Plasmid pSL553 (pRS313, p_{ROD1}:*ROD1*-NcoI-Flag) was generated by site-directed mutagenesis on pSL234
491 (pRS313-based, p_{ROD1}:*ROD1*-Flag, a kind gift of O. Vincent, CSIC, Madrid, Spain) to integrate a NcoI site
492 between *ROD1* and the Flag-tag, allowing to substitute the WT ORF of *ROD1* by mutated versions at SalI-NcoI
493 sites as follows. The inserts p_{ROD1}:*ROD1*-WT-Flag (pSL559), p_{ROD1}:*ROD1-PYm*-Flag (pSL560) p_{ROD1}:*ROD1-S12A*-
494 Flag (pSL561) and p_{ROD1}:*ROD1-KR*-Flag (pSL563) were PCR amplified (oSL1662/oSL1663) using as templates
495 pSL94 (p_{ROD1}:*ROD1*-3HA) [28], pSL119 (p_{ROD1}:*ROD1-PYm*-3HA) [28], pSL152 (p_{ROD1}:*ROD1-S12A*-3HA) (see
496 below), and pSL147 (p_{ROD1}:*ROD1-KR*-3HA, carrying mutations K235R, K245R, K264R, K267R) [28] respectively.
497 They were digested with SalI/NcoI and cloned at these sites into pSL553 (p_{ROD1}:*ROD1*-NcoI-Flag). Plasmid
498 pSL152 (pRS415, p_{ROD1}-ROD1(S12A)-3HA) was made from a synthetic gene designed to mutate S125, S138,
499 S315, S358, S447, S623, S641, S706, S720, S734, S781, and S821 residues into A (Eurofins), digested
500 PacI/XmaI and cloned PacI/XmaI into pSL94 at the place of WT *ROD1* (pRS415, p_{ROD1}:*ROD1*-3HA) [28].
501 To construct pSL589 (pUG35-based, p_{HXT3}-Hxt3-GFP), the *HXT3* promoter (1kb) was first cloned into pUG35
502 after amplification by PCR on WT gDNA (oSL1739/oSL1740) at BamHI/SpeI sites to give pSL592. The *HXT3-*
503 *GFP* ORF was PCR-amplified (oSL1770/oSL1771) from gDNA of the Hxt3-GFP strain (ySL1027) using primers
504 overlapping with the pSL592 sequence and cloned into pSL592 by gap-repair, and later rescued in bacteria to
505 obtain pSL589. The N367A mutation was introduced using 2 overlapping PCR products amplified from gDNA
506 of the HXT3-GFP strain (ySL1027) (oSL1730/oSL682 and oSL1731/oSL1563) and cloned by gap-repair into
507 pSL592 to give pSL591. Plasmid pSL599 (pRS426, p_{HXT1}:*HXT1*) was obtained by (1) amplifying the *HXT1* gene (-
508 515/+225) from WT genomic DNA (oSL435/oSL932) into a pCRII-blunt topo vector (pSL597), (2) cloning a
509 BamHI/XhoI fragment of pSL597 into pRS425 at BamHI/XhoI sites. For plasmid pSL602 (pRS426, p_{HXT1}:*HXT1*),
510 A PCR amplifying the *HXT3* gene (and 1kb of promoter) was obtained from WT genomic DNA
511 (oSL1739/oSL1734), digested BamhI/SpeI and cloned BamHI/SpeI in pRS426.
512 All constructs were verified by sequencing.
513

514 **Total protein extracts and immunoblotting**

515 Yeast were always grown in SC medium. For each protein sample, 1.4 ml of culture was incubated with 140µl
516 of 100% TCA for 10 min on ice to precipitate proteins, centrifuged at 16,000g at 4°C for 10 min, and broken
517 for 10 min with glass beads. Lysates were transferred to another 1.5-ml tube to remove glass beads and
518 centrifuged for 5 min at 16,000g at 4°C, supernatants were discarded, and protein pellets were resuspended
519 in sample buffer [50 mM tris-HCl (pH 6.8), 100 mM dithiothreitol, 2% SDS, 0.1% bromophenol blue, and 10%

520 glycerol, complemented with 50 mM tris-base (pH 8.8)] (50µl/initial OD). Protein samples were heated at
521 37°C for 5 min and 10 µl was loaded on SDS–polyacrylamide gel electrophoresis (PAGE) gels (4-20% Mini-
522 PROTEAN TGX Stain-Free, Bio-Rad). After electrophoresis for 30 min at 200V, total proteins were visualized
523 by in-gel fluorescence using a trihalo compound incorporated in SDS–PAGE gels (stain-free TGX gels, 4–20%;
524 Bio-Rad) after 45 sec UV-induced photoactivation using a ChemiDoc MP imager (BioRad), serving as a loading
525 control. Gels were transferred on nitrocellulose membranes for 60 min (100V) in a liquid transfer system
526 (Bio-Rad). Membranes were blocked in Tris-buffered saline solution containing 0.5% Tween-20 (TBS-T) and
527 2% milk for 30 min and incubated for at least 2 hours with the corresponding primary antibodies.
528 Membranes were washed 3x10 min in TBS-T and incubated for at least an hour with the corresponding
529 secondary antibody (coupled with horseradish peroxidase). Membranes were then washed again 3x10 min in
530 TBS-T and incubated with SuperSignal West Femto reagent (Thermo). Luminescence signals were acquired
531 using a ChemiDoc MP (BioRad). Primary and secondary antibodies used in this study as well as their dilutions
532 are listed in table S3.
533
534 **Treatment of protein extracts with calf intestinal phosphatase (CIP) or Endoglycosidase H (EndoH)**
535 Calf Intestine Phosphatase (CIP, Roche ref 11097075001) was used to dephosphorylate proteins prior to
536 electrophoresis. Samples were prepared using 20 µL of TCA protein extract (see "Protein extracts and
537 immunoblotting", above), to which 2 µL of 10X CIP buffer supplied with the enzyme, as well as 0.6 µL of 1.5M
538 Tris pH 8.8, 0.2 µL 0.1M $MgSO_4$, and 17.2 µL of H_2O were added. The extract was split in 2 and 0.6 U CIP was
539 added to one of the samples. Samples were incubated at 37°C for 3 h, and loaded on SDS-PAGE.
540 Endoglycosidase H (EndoH) (Promega V4871, 500 U/µL) was used to deglycosylate Ina1-GFP-containing
541 samples. Samples were prepared using 10 µL of TCA protein extract (see "Protein extracts and
542 immunoblotting", above) to which 2 µL of the supplied buffer, 1 µL of EndoH and 7 µL of water were added.
543 A control sample without EndoH was also prepared. Samples were incubated for 2 h at 37°C and loaded on
544 SDS-PAGE.
545
546 **Beta-galactosidase assays**
547 Beta-galactosidase assays were performed using 1 ml of mid-log phase yeast cultures carrying the *pDOG1-*
548 *LacZ* (pSL409) or *pDOG2-LacZ* plasmids (pSL410) [20], grown overnight to the mid-log phase in SC medium
549 without uracil with 2% glucose and switched to the specified conditions. The OD(600 nm) of the culture was
550 measured, and samples were taken and centrifuged at 16,000g at 4°C for 10 min. Cell pellets were snap-
551 frozen in liquid nitrogen and resuspended in 800 µl of buffer Z (pH 7, 50 mM NaH_2PO_4, 45 mM Na_2HPO_4, 10
552 mM $MgSO_4$, 10 mM KCl, and 38 mM beta-mercaptoethanol). After addition of 160µl of ONPG (ortho-
553 nitrophenyl-d-galactopyranoside, 4 mg/ml; Sigma-Aldrich), samples were incubated at 37°C. Enzymatic
554 reactions were stopped in the linear phase (60-min incubation for *pDOG2-LacZ* and 120-min incubation for
555 the *pDOG1-LacZ* plasmid, as per initial tests) [20] by addition of 400 µl of Na_2CO_3, and cell debris were
556 discarded by centrifugation at 16,000g. The absorbance of clarified samples was measured with a
557 spectrophotometer set at 420 nm.
558 Galactosidase activities (arbitrary units) were calculated using the formula 1000*[A420/(A600*t)], where
559 A420 refers to the measured enzyme activity, A600 is the turbidity of the culture, and t is the incubation
560 time. Each enzymatic assay was repeated independently at least three times.
561
562 **2DG-6-phosphate assays**
563 Cells were grown overnight in SC media until mid-log phase. 2DG was added into the culture to a final
564 concentration of 0.2% for the indicated time. For the chase experiments, the cultures were centrifuged after
565 2 hours, washed with water and re-suspended in the same volume of SC medium without 2DG. For each time
566 points, 1 OD equivalent of cells were taken, immediately placed on ice, centrifuged at 4°C for 4' at 16,000g,
567 washed once with cold PBS and lysed using Y-PER Yeast Protein Extraction Reagent (ThermoFisher Scientific)

568 as previously described [85]. Briefly, 1 OD equivalent of cells was resuspended in 100µL of Y-PER buffer,
569 incubated for 20' at 30°C, and centrifuged for 4' at 16100g at room temperature. The supernatant (between
570 0.0125 and 0.0625 OD equivalents) was used for the assay and diluted in Y-PER when needed. The assay was
571 performed using the 2DG uptake measurement kit (Cosmo Bio USA, Carlsbad, CA, USA;, Ref. CSR-OKP-PMG-
572 K01H) following the manufacturer's protocol adapted for a total reaction volume of 100 µL. Absorbance at
573 420 nm was measured every minute for 1 hour on a SpectraMax M2 Microplate Reader (Molecular Devices).
574 Measures taken between 20 and 35 minutes (linear range) were taken into account to compare the slopes.
575 Each sample was assayed at least twice in each experiment and at least three independent experiments were
576 performed. Mean values were calculated and were plotted with error bars representing SEM. Statistical
577 significance was determined using a *t*-test for paired variables assuming a normal distribution of the values
578 (unless otherwise stated) using GraphPad Prism7.
579
580 **Glucose FRET sensor experiments**
581 Yeast transformed with the plasmid FLII12Pglu-700µδ6 (pSL590, [a gift from Wolf Frommer: Addgene
582 #28002, 59] were grown overnight in SC-URA medium to reach an OD600nm of 0.3-0.7 in the morning. Cells
583 were centrifuged at 3000g for 5 minutes and the cell pellets were resuspended in 20mM MES pH=6 to a final
584 OD of 0.6. 180µl of the cell suspension were distributed in 12 wells of a 96-well black PS microplate with flat
585 bottom (Greiner). Fluorescence was measured with a plate reader (Spark, TECAN) set at 30°C before the
586 experiment was started.
587 A first measurement for 3 cycles was performed to establish a baseline (each cycle is around 90 seconds with
588 10 seconds shaking before each measurement of the fluorescence). Cells were excited at CFP wavelength
589 excitation (428 nm) and the emission intensities at 485 nm (CFP) and 528 nm (Citrine) were collected. The
590 cycle was then paused to inject 20µl of the glucose solutions using a multichannel pipette, and the plate
591 rapidly reloaded in the reader to restart measurements for another 17 cycles. Data were collected and
592 analyzed in an Excel spreadsheet and in Prism 7.0 (GraphPad). Emission intensity values of yeast transformed
593 with an empty plasmid were subtracted from emissions values at 485 nm and 528 nm for each measurement
594 at the different glucose concentrations. The emission intensity ratio for Citrine (528 nm) over CFP (485 nm)
595 was calculated. All analyses were repeated (with three technical replicates) at least three times
596 independently. Emission ratios were normalized to the average of the three initial ratio values before glucose
597 addition.
598
599 **ATP FRET sensor experiments**
600 Yeast transformed with the plasmid pDRF1-GW yAT1.03 (pSL608) [a gift from Bas Teusink: Addgene #132781,
601 49] were grown overnight in SC-URA medium to reach an OD600nm of 0.3-0.7 in the morning. FRET
602 measurements were performed as above except cells were excited at 438 nm and the emission intensities at
603 483 nm (ymTq2Δ11) and 593nm (tdTomato) were collected. A plasmid encoding a mutated sensor which
604 does not bind ATP (pSL609) [a gift from Bas Teusink: Addgene #132782, 49] was used as a negative control.
605
606 **Drop tests**
607 Yeast cells grown in liquid-rich or SC medium for at least 6 hours at 30°C were adjusted to an optical density
608 (600 nm) of 1. Serial 10-fold dilutions were prepared in 96-well plates and spotted on plates containing rich
609 or SC medium containing 2% (w/v) agar and, when indicated, 2DG [0.05 or 0.2% (w/v)]. Plates were
610 incubated at 30°C for 3 to 4 days before scanning on a desktop scanner (Epson).
611
612 **Microscopy**
613 Cells were mounted in synthetic complete medium with the appropriate carbon source and observed with a
614 motorized Olympus BX-61 fluorescence microscope equipped with an Olympus PlanApo 100× oil-immersion
615 objective (1.40 NA), a Spot 4.05 charge-coupled device camera and the MetaVue acquisition software

616 (Molecular Devices; Sunnyvale, CA) and imaged at room temperature. GFP-tagged proteins were visualized
617 using a Chroma GFP II filter (excitation 440–470 nm). mCherry-tagged proteins were visualized using an
618 HcRed I filter (excitation 525–575 nm). Images were processed in ImageJ (NIH). Vacuolar staining was
619 obtained by incubating cells grown in the desired condition with 100 µM CMAC (Life Technologies) for 10 min
620 under agitation at 30°C. Cells are then washed twice with water before observations with a fluorescence
621 microscope equipped with a DAPI filter.
622
623 **Quantification of vacuolar fragmentation**
624 Quantification of vacuolar fragmentation (Fig. S1B) was performed with ImageJ. For each experiment and
625 each strain, at least 30 cells were observed and the quantification was done blindly. Cells with more than 3
626 vacuoles were considered as cells with highly fragmented vacuoles.
627
628 **Quantification of Western-blots**
629 Western blot quantifications were performed with ImageJ. The integrated density of proteins of interest was
630 divided by the integrated density of total proteins. Results were normalized to the Glc ON condition of each
631 protein. The ratio of undegraded protein is shown. The experiments were repeated three times. Datas were
632 analyzed and processed with Prism7 software (GraphPad). The statistical test performed was a one-way
633 analysis of variance (ANOVA) test.
634
635 **Statistical analysis**
636 Mean values were calculated using a minimum of three independent measurements from three biological
637 replicates and were plotted with error bars representing SEM. Statistical significance was determined using a
638 *t*-test for paired variables assuming a normal distribution of the values using GraphPad Prism7.
639

640 ## References

641 1. Xi H, Kurtoglu M, Lampidis TJ. The wonders of 2-deoxy-D-glucose. IUBMB Life. 2014;66(2):110-21. Epub
642 2014/03/01. doi: 10.1002/iub.1251. PubMed PMID: 24578297.
643 2. Hardie DG. Regulation of AMP-activated protein kinase by natural and synthetic activators. Acta Pharm
644 Sin B. 2016;6(1):1-19. doi: 10.1016/j.apsb.2015.06.002. PubMed PMID: 26904394; PubMed Central
645 PMCID: PMCPMC4724661.
646 3. Laussel C, Leon S. Cellular toxicity of the metabolic inhibitor 2-deoxyglucose and associated resistance
647 mechanisms. Biochem Pharmacol. 2020;182:114213. doi: 10.1016/j.bcp.2020.114213. PubMed PMID:
648 32890467.
649 4. Kurtoglu M, Gao N, Shang J, Maher JC, Lehrman MA, Wangpaichitr M, et al. Under normoxia, 2-deoxy-D-
650 glucose elicits cell death in select tumor types not by inhibition of glycolysis but by interfering with N-
651 linked glycosylation. Molecular cancer therapeutics. 2007;6(11):3049-58. Epub 2007/11/21. doi:
652 10.1158/1535-7163.MCT-07-0310. PubMed PMID: 18025288.
653 5. Luengo A, Gui DY, Vander Heiden MG. Targeting Metabolism for Cancer Therapy. Cell Chem Biol.
654 2017;24(9):1161-80. doi: 10.1016/j.chembiol.2017.08.028. PubMed PMID: 28938091; PubMed Central
655 PMCID: PMCPMC5744685.
656 6. Pajak B, Siwiak E, Soltyka M, Priebe A, Zielinski R, Fokt I, et al. 2-Deoxy-d-Glucose and Its Analogs: From
657 Diagnostic to Therapeutic Agents. Int J Mol Sci. 2019;21(1). doi: 10.3390/ijms21010234. PubMed PMID:
658 31905745; PubMed Central PMCID: PMCPMC6982256.
659 7. Kayikci O, Nielsen J. Glucose repression in Saccharomyces cerevisiae. FEMS Yeast Res. 2015;15(6):fov068.
660 doi: 10.1093/femsyr/fov068. PubMed PMID: 26205245; PubMed Central PMCID: PMCPMC4629793.
661 8. Coccetti P, Nicastro R, Tripodi F. Conventional and emerging roles of the energy sensor Snf1/AMPK in
662 Saccharomyces cerevisiae. Microb Cell. 2018;5(11):482-94. doi: 10.15698/mic2018.11.655. PubMed
663 PMID: 30483520; PubMed Central PMCID: PMCPMC6244292.
664 9. De Vit MJ, Waddle JA, Johnston M. Regulated nuclear translocation of the Mig1 glucose repressor.
665 Molecular Biology of the Cell. 1997;8(8):1603-18. PubMed PMID: 9285828; PubMed Central PMCID:
666 PMCPMC276179.
667 10. Papamichos-Chronakis M, Gligoris T, Tzamarias D. The Snf1 kinase controls glucose repression in yeast by
668 modulating interactions between the Mig1 repressor and the Cyc8-Tup1 co-repressor. EMBO Rep.
669 2004;5(4):368-72. doi: 10.1038/sj.embor.7400120. PubMed PMID: 15031717; PubMed Central PMCID:
670 PMCPMC1299031.
671 11. McCartney RR, Schmidt MC. Regulation of Snf1 kinase. Activation requires phosphorylation of threonine
672 210 by an upstream kinase as well as a distinct step mediated by the Snf4 subunit. The Journal of
673 biological chemistry. 2001;276(39):36460-6. doi: 10.1074/jbc.M104418200. PubMed PMID: 11486005.
674 12. Rubenstein EM, McCartney RR, Zhang C, Shokat KM, Shirra MK, Arndt KM, et al. Access denied: Snf1
675 activation loop phosphorylation is controlled by availability of the phosphorylated threonine 210 to the
676 PP1 phosphatase. J Biol Chem. 2008;283(1):222-30. Epub 2007/11/10. doi: 10.1074/jbc.M707957200.
677 PubMed PMID: 17991748.
678 13. Tu J, Carlson M. REG1 binds to protein phosphatase type 1 and regulates glucose repression in
679 Saccharomyces cerevisiae. EMBO J. 1995;14(23):5939-46. Epub 1995/12/01. PubMed PMID: 8846786;
680 PubMed Central PMCID: PMCPMC394713.
681 14. Ralser M, Wamelink MM, Struys EA, Joppich C, Krobitsch S, Jakobs C, et al. A catabolic block does not
682 sufficiently explain how 2-deoxy-D-glucose inhibits cell growth. Proc Natl Acad Sci U S A.
683 2008;105(46):17807-11. doi: 10.1073/pnas.0803090105. PubMed PMID: 19004802; PubMed Central
684 PMCID: PMC2584745.

685 15. Schmidt MC, O'Donnell AF. 'Sugarcoating' 2-deoxyglucose: mechanisms that suppress its toxic effects.
686 Current genetics. 2021;67(1):107-14. doi: 10.1007/s00294-020-01122-7. PubMed PMID: 33136227.
687 16. McCartney RR, Chandrashekarappa DG, Zhang BB, Schmidt MC. Genetic analysis of resistance and
688 sensitivity to 2-deoxyglucose in Saccharomyces cerevisiae. Genetics. 2014;198(2):635-46. doi:
689 10.1534/genetics.114.169060. PubMed PMID: 25116136; PubMed Central PMCID: PMC4196618.
690 17. Barban S. Studies on the mechanism of resistance to 2-deoxy-D-glucose in mammalian cell cultures. J Biol
691 Chem. 1962;237:291-5. Epub 1962/02/01. PubMed PMID: 13864809.
692 18. Sanz P, Randez-Gil F, Prieto JA. Molecular characterization of a gene that confers 2-deoxyglucose
693 resistance in yeast. Yeast. 1994;10(9):1195-202. Epub 1994/09/01. doi: 10.1002/yea.320100907. PubMed
694 PMID: 7754708.
695 19. Randez-Gil F, Blasco A, Prieto JA, Sanz P. DOGR1 and DOGR2: two genes from Saccharomyces cerevisiae
696 that confer 2-deoxyglucose resistance when overexpressed. Yeast. 1995;11(13):1233-40. Epub
697 1995/10/01. doi: 10.1002/yea.320111303. PubMed PMID: 8553694.
698 20. Defenouillère Q, Verraes A, Laussel C, Friedrich A, Schacherer J, Leon S. The induction of HAD-like
699 phosphatases by multiple signaling pathways confers resistance to the metabolic inhibitor 2-
700 deoxyglucose. Sci Signal. 2019;12(597):aaw8000. doi: 10.1126/scisignal.aaw8000. PubMed PMID:
701 31481524.
702 21. Soncini SR, Chandrashekarappa DG, Augustine DA, Callahan KP, O'Donnell AF, Schmidt MC. Spontaneous
703 mutations that confer resistance to 2-deoxyglucose act through Hxk2 and Snf1 pathways to regulate gene
704 expression and HXT endocytosis. PLoS Genet. 2020;16(7):e1008484. doi: 10.1371/journal.pgen.1008484.
705 PubMed PMID: 32673313; PubMed Central PMCID: PMCPMC7386655.
706 22. Barney JB, Chandrashekarappa DG, Soncini SR, Schmidt MC. Drug resistance in diploid yeast is acquired
707 through dominant alleles, haploinsufficiency, gene duplication and aneuploidy. PLoS Genet.
708 2021;17(9):e1009800. doi: 10.1371/journal.pgen.1009800. PubMed PMID: 34555030; PubMed Central
709 PMCID: PMCPMC8460028.
710 23. Piper RC, Dikic I, Lukacs GL. Ubiquitin-dependent sorting in endocytosis. Cold Spring Harb Perspect Biol.
711 2014;6(1). Epub 2014/01/05. doi: 10.1101/cshperspect.a016808. PubMed PMID: 24384571; PubMed
712 Central PMCID: PMCPMC3941215.
713 24. MacGurn JA, Hsu PC, Emr SD. Ubiquitin and membrane protein turnover: from cradle to grave. Annu Rev
714 Biochem. 2012;81:231-59. Epub 2012/03/13. doi: 10.1146/annurev-biochem-060210-093619. PubMed
715 PMID: 22404628.
716 25. Sardana R, Emr SD. Membrane Protein Quality Control Mechanisms in the Endo-Lysosome System. Trends
717 Cell Biol. 2021;31(4):269-83. doi: 10.1016/j.tcb.2020.11.011. PubMed PMID: 33414051.
718 26. Babst M. Regulation of nutrient transporters by metabolic and environmental stresses. Curr Opin Cell Biol.
719 2020;65:35-41. doi: 10.1016/j.ceb.2020.02.009. PubMed PMID: 32200208; PubMed Central PMCID:
720 PMCPMC7501145.
721 27. Kahlhofer J, Leon S, Teis D, Schmidt O. The alpha-arrestin family of ubiquitin ligase adaptors links
722 metabolism with selective endocytosis. Biology of the cell / under the auspices of the European Cell
723 Biology Organization. 2021;113(4):183-219. Epub 2020/12/15. doi: 10.1111/boc.202000137. PubMed
724 PMID: 33314196.
725 28. Becuwe M, Vieira N, Lara D, Gomes-Rezende J, Soares-Cunha C, Casal M, et al. A molecular switch on an
726 arrestin-like protein relays glucose signaling to transporter endocytosis. J Cell Biol. 2012;196(2):247-59.
727 Epub 2012/01/18. doi: 10.1083/jcb.201109113. PubMed PMID: 22249293.
728 29. Llopis-Torregrosa V, Ferri-Blazquez A, Adam-Artigues A, Deffontaines E, van Heusden GP, Yenush L.
729 Regulation of the Yeast Hxt6 Hexose Transporter by the Rod1 alpha-Arrestin, the Snf1 Protein Kinase, and
730 the Bmh2 14-3-3 Protein. J Biol Chem. 2016;291(29):14973-85. doi: 10.1074/jbc.M116.733923. PubMed
731 PMID: 27261460; PubMed Central PMCID: PMC4946916.

30. O'Donnell AF, Schmidt MC. AMPK-Mediated Regulation of Alpha-Arrestins and Protein Trafficking. Int J Mol Sci. 2019;20(3). Epub 2019/01/30. doi: 10.3390/ijms20030515. PubMed PMID: 30691068; PubMed Central PMCID: PMCPMC6387238.
31. Shinoda J, Kikuchi Y. Rod1, an arrestin-related protein, is phosphorylated by Snf1-kinase in *Saccharomyces cerevisiae*. Biochem Biophys Res Commun. 2007;364(2):258-63. Epub 2007/10/24. doi: 10.1016/j.bbrc.2007.09.134. PubMed PMID: 17949685.
32. O'Donnell AF, McCartney RR, Chandrashekarappa DG, Zhang BB, Thorner J, Schmidt MC. 2-Deoxyglucose impairs *Saccharomyces cerevisiae* growth by stimulating Snf1-regulated and alpha-arrestin-mediated trafficking of hexose transporters 1 and 3. Mol Cell Biol. 2015;35(6):939-55. doi: 10.1128/MCB.01183-14. PubMed PMID: 25547292; PubMed Central PMCID: PMCPMC4333089.
33. Yang X, Reist L, Chomchai DA, Chen L, Arines FM, Li M. ESCRT, not intralumenal fragments, sorts ubiquitinated vacuole membrane proteins for degradation. J Cell Biol. 2021;220(8). doi: 10.1083/jcb.202012104. PubMed PMID: 34047770; PubMed Central PMCID: PMCPMC8167898.
34. Stauffer B, Powers T. Target of rapamycin signaling mediates vacuolar fission caused by endoplasmic reticulum stress in Saccharomyces cerevisiae. Mol Biol Cell. 2015;26(25):4618-30. Epub 2015/10/16. doi: 10.1091/mbc.E15-06-0344. PubMed PMID: 26466677; PubMed Central PMCID: PMCPMC4678019.
35. Becuwe M, Leon S. Integrated control of transporter endocytosis and recycling by the arrestin-related protein Rod1 and the ubiquitin ligase Rsp5. eLife. 2014;3:03307. doi: 10.7554/eLife.03307. PubMed PMID: 25380227; PubMed Central PMCID: PMC4244573.
36. Alvaro CG, Aindow A, Thorner J. Differential Phosphorylation Provides a Switch to Control How alpha-Arrestin Rod1 Down-regulates Mating Pheromone Response in Saccharomyces cerevisiae. Genetics. 2016;203(1):299-317. Epub 2016/02/28. doi: 10.1534/genetics.115.186122. PubMed PMID: 26920760; PubMed Central PMCID: PMCPMC4858781.
37. Alvaro CG, O'Donnell AF, Prosser DC, Augustine AA, Goldman A, Brodsky JL, et al. Specific alpha-arrestins negatively regulate *Saccharomyces cerevisiae* pheromone response by down-modulating the G-protein-coupled receptor Ste2. Mol Cell Biol. 2014;34(14):2660-81. doi: 10.1128/MCB.00230-14. PubMed PMID: 24820415; PubMed Central PMCID: PMCPMC4097657.
38. Germann SM, Schramke V, Pedersen RT, Gallina I, Eckert-Boulet N, Oestergaard VH, et al. TopBP1/Dpb11 binds DNA anaphase bridges to prevent genome instability. J Cell Biol. 2014;204(1):45-59. doi: 10.1083/jcb.201305157. PubMed PMID: 24379413; PubMed Central PMCID: PMCPMC3882784.
39. Vincent EE, Coelho PP, Blagih J, Griss T, Viollet B, Jones RG. Differential effects of AMPK agonists on cell growth and metabolism. Oncogene. 2015;34(28):3627-39. doi: 10.1038/onc.2014.301. PubMed PMID: 25241895; PubMed Central PMCID: PMCPMC4980123.
40. Orlova M, Barrett L, Kuchin S. Detection of endogenous Snf1 and its activation state: application to Saccharomyces and Candida species. Yeast. 2008;25(10):745-54. doi: 10.1002/yea.1628. PubMed PMID: 18949820.
41. Smith FC, Davies SP, Wilson WA, Carling D, Hardie DG. The SNF1 kinase complex from Saccharomyces cerevisiae phosphorylates the transcriptional repressor protein Mig1p in vitro at four sites within or near regulatory domain 1. FEBS Lett. 1999;453(1-2):219-23. doi: 10.1016/s0014-5793(99)00725-5. PubMed PMID: 10403407.
42. Treitel MA, Kuchin S, Carlson M. Snf1 protein kinase regulates phosphorylation of the Mig1 repressor in Saccharomyces cerevisiae. Mol Cell Biol. 1998;18(11):6273-80. Epub 1998/10/17. PubMed PMID: 9774644; PubMed Central PMCID: PMCPMC109214.
43. Shashkova S, Wollman AJM, Leake MC, Hohmann S. The yeast Mig1 transcriptional repressor is dephosphorylated by glucose-dependent and -independent mechanisms. FEMS Microbiol Lett. 2017;364(14). Epub 2017/09/01. doi: 10.1093/femsle/fnx133. PubMed PMID: 28854669.

44. van Steveninck J. Transport-associated phosphorylation of 2-deoxy-D-glucose in yeast. Biochim Biophys Acta. 1968;163(3):386-94. Epub 1968/11/05. doi: 10.1016/0005-2736(68)90123-5. PubMed PMID: 5721900.
45. Herrero P, Galindez J, Ruiz N, Martinez-Campa C, Moreno F. Transcriptional regulation of the Saccharomyces cerevisiae HXK1, HXK2 and GLK1 genes. Yeast. 1995;11(2):137-44. doi: 10.1002/yea.320110205. PubMed PMID: 7732723.
46. Saito K, Lee S, Shiuchi T, Toda C, Kamijo M, Inagaki-Ohara K, et al. An enzymatic photometric assay for 2-deoxyglucose uptake in insulin-responsive tissues and 3T3-L1 adipocytes. Anal Biochem. 2011;412(1):9-17. doi: 10.1016/j.ab.2011.01.022. PubMed PMID: 21262191.
47. Karczmar GS, Arbeit JM, Toy BJ, Speder A, Weiner MW. Selective depletion of tumor ATP by 2-deoxyglucose and insulin, detected by 31P magnetic resonance spectroscopy. Cancer Res. 1992;52(1):71-6. Epub 1992/01/01. PubMed PMID: 1727388.
48. Ibanez AJ, Fagerer SR, Schmidt AM, Urban PL, Jefimovs K, Geiger P, et al. Mass spectrometry-based metabolomics of single yeast cells. Proc Natl Acad Sci U S A. 2013;110(22):8790-4. doi: 10.1073/pnas.1209302110. PubMed PMID: 23671112; PubMed Central PMCID: PMCPMC3670324.
49. Botman D, van Heerden JH, Teusink B. An Improved ATP FRET Sensor For Yeast Shows Heterogeneity During Nutrient Transitions. ACS Sens. 2020;5(3):814-22. doi: 10.1021/acssensors.9b02475. PubMed PMID: 32077276; PubMed Central PMCID: PMCPMC7106129.
50. Ozcan S, Johnston M. Function and regulation of yeast hexose transporters. Microbiol Mol Biol Rev. 1999;63(3):554-69. doi: 10.1042/bj3630737. PubMed PMID: 10477308; PubMed Central PMCID: PMCPMC103746.
51. Yan N. A Glimpse of Membrane Transport through Structures-Advances in the Structural Biology of the GLUT Glucose Transporters. J Mol Biol. 2017;429(17):2710-25. doi: 10.1016/j.jmb.2017.07.009. PubMed PMID: 28756087.
52. Mueckler M, Makepeace C. Model of the exofacial substrate-binding site and helical folding of the human Glut1 glucose transporter based on scanning mutagenesis. Biochemistry. 2009;48(25):5934-42. doi: 10.1021/bi900521n. PubMed PMID: 19449892; PubMed Central PMCID: PMCPMC2776625.
53. Deng D, Xu C, Sun P, Wu J, Yan C, Hu M, et al. Crystal structure of the human glucose transporter GLUT1. Nature. 2014;510(7503):121-5. doi: 10.1038/nature13306. PubMed PMID: 24847886.
54. Farwick A, Bruder S, Schadeweg V, Oreb M, Boles E. Engineering of yeast hexose transporters to transport D-xylose without inhibition by D-glucose. Proc Natl Acad Sci U S A. 2014;111(14):5159-64. doi: 10.1073/pnas.1323464111. PubMed PMID: 24706835; PubMed Central PMCID: PMCPMC3986176.
55. Nijland JG, Shin HY, de Jong RM, de Waal PP, Klaassen P, Driessen AJ. Engineering of an endogenous hexose transporter into a specific D-xylose transporter facilitates glucose-xylose co-consumption in Saccharomyces cerevisiae. Biotechnol Biofuels. 2014;7(1):168. doi: 10.1186/s13068-014-0168-9. PubMed PMID: 25505932; PubMed Central PMCID: PMCPMC4263072.
56. Shin HY, Nijland JG, de Waal PP, de Jong RM, Klaassen P, Driessen AJ. An engineered cryptic Hxt11 sugar transporter facilitates glucose-xylose co-consumption in Saccharomyces cerevisiae. Biotechnol Biofuels. 2015;8:176. doi: 10.1186/s13068-015-0360-6. PubMed PMID: 26535057; PubMed Central PMCID: PMCPMC4630928.
57. Roy A, Dement AD, Cho KH, Kim JH. Assessing glucose uptake through the yeast hexose transporter 1 (Hxt1). PLoS One. 2015;10(3):e0121985. doi: 10.1371/journal.pone.0121985. PubMed PMID: 25816250; PubMed Central PMCID: PMC4376911.
58. Nijland JG, Li X, Shin HY, de Waal PP, Driessen AJM. Efficient, D-glucose insensitive, growth on D-xylose by an evolutionary engineered Saccharomyces cerevisiae strain. FEMS Yeast Res. 2019;19(8). doi: 10.1093/femsyr/foz083. PubMed PMID: 31782779.

824 59. Bermejo C, Haerizadeh F, Takanaga H, Chermak D, Frommer WB. Dynamic analysis of cytosolic glucose
825 and ATP levels in yeast using optical sensors. Biochem J. 2010;432(2):399-406. doi: 10.1042/BJ20100946.
826 PubMed PMID: 20854260; PubMed Central PMCID: PMC2992555.
827 60. Fehr M, Lalonde S, Lager I, Wolff MW, Frommer WB. In vivo imaging of the dynamics of glucose uptake in
828 the cytosol of COS-7 cells by fluorescent nanosensors. J Biol Chem. 2003;278(21):19127-33. Epub
829 20030320. doi: 10.1074/jbc.M301333200. PubMed PMID: 12649277.
830 61. Lang MJ, Martinez-Marquez JY, Prosser DC, Ganser LR, Buelto D, Wendland B, et al. Glucose starvation
831 inhibits autophagy via vacuolar hydrolysis and induces plasma membrane internalization by down-
832 regulating recycling. J Biol Chem. 2014;289(24):16736-47. doi: 10.1074/jbc.M113.525782. PubMed PMID:
833 24753258; PubMed Central PMCID: PMC4059118.
834 62. Müller M, Schmidt O, Angelova M, Faserl K, Weys S, Kremser L, et al. The coordinated action of the MVB
835 pathway and autophagy ensures cell survival during starvation. eLife. 2015;4:e07736. doi:
836 10.7554/eLife.07736. PubMed PMID: 25902403; PubMed Central PMCID: PMCPMC4424281.
837 63. Ivashov V, Zimmer J, Schwabl S, Kahlhofer J, Weys S, Gstir R, et al. Complementary alpha-arrestin-
838 ubiquitin ligase complexes control nutrient transporter endocytosis in response to amino acids. eLife.
839 2020;9. doi: 10.7554/eLife.58246. PubMed PMID: 32744498.
840 64. Volland C, Urban-Grimal D, Geraud G, Haguenauer-Tsapis R. Endocytosis and degradation of the yeast
841 uracil permease under adverse conditions. J Biol Chem. 1994;269(13):9833-41. Epub 1994/04/01.
842 PubMed PMID: 8144575.
843 65. MacGurn JA, Hsu PC, Smolka MB, Emr SD. TORC1 regulates endocytosis via Npr1-mediated
844 phosphoinhibition of a ubiquitin ligase adaptor. Cell. 2011;147(5):1104-17. Epub 2011/11/29. doi:
845 10.1016/j.cell.2011.09.054. PubMed PMID: 22118465.
846 66. Nikko E, Pelham HR. Arrestin-mediated endocytosis of yeast plasma membrane transporters. Traffic.
847 2009;10(12):1856-67. Epub 2009/11/17. doi: 10.1111/j.1600-0854.2009.00990.x. PubMed PMID:
848 19912579.
849 67. Megarioti AH, Primo C, Kapetanakis GC, Athanasopoulos A, Sophianopoulou V, Andre B, et al. The Bul1/2
850 Alpha-Arrestins Promote Ubiquitylation and Endocytosis of the Can1 Permease upon Cycloheximide-
851 Induced TORC1-Hyperactivation. Int J Mol Sci. 2021;22(19). doi: 10.3390/ijms221910208. PubMed PMID:
852 34638549; PubMed Central PMCID: PMCPMC8508209.
853 68. Crapeau M, Merhi A, Andre B. Stress Conditions Promote Yeast Gap1 Permease Ubiquitylation and Down-
854 regulation via the Arrestin-like Bul and Aly Proteins. J Biol Chem. 2014;289(32):22103-16. doi:
855 10.1074/jbc.M114.582320. PubMed PMID: 24942738; PubMed Central PMCID: PMC4139224.
856 69. Zhao Y, Macgurn JA, Liu M, Emr S. The ART-Rsp5 ubiquitin ligase network comprises a plasma membrane
857 quality control system that protects yeast cells from proteotoxic stress. eLife. 2013;2:e00459. doi:
858 10.7554/eLife.00459. PubMed PMID: 23599894; PubMed Central PMCID: PMC3628405.
859 70. Merhi A, André B. Internal amino acids promote Gap1 permease ubiquitylation via TORC1/Npr1/14-3-3-
860 dependent control of the Bul arrestin-like adaptors. Mol Cell Biol. 2012;32(22):4510-22. Epub 2012/09/12.
861 doi: 10.1128/mcb.00463-12. PubMed PMID: 22966204; PubMed Central PMCID: PMC3486192.
862 71. Lee S, Ho HC, Tumolo JM, Hsu PC, MacGurn JA. Methionine triggers Ppz-mediated dephosphorylation of
863 Art1 to promote cargo-specific endocytosis. J Cell Biol. 2019;218(3):977-92. doi: 10.1083/jcb.201712144.
864 PubMed PMID: 30610170; PubMed Central PMCID: PMCPMC6400557.
865 72. Lin CH, MacGurn JA, Chu T, Stefan CJ, Emr SD. Arrestin-related ubiquitin-ligase adaptors regulate
866 endocytosis and protein turnover at the cell surface. Cell. 2008;135(4):714-25. Epub 2008/11/04. doi:
867 10.1016/j.cell.2008.09.025. PubMed PMID: 18976803.
868 73. MacDonald C, Shields SB, Williams CA, Winistorfer S, Piper RC. A Cycle of Ubiquitination Regulates
869 Adaptor Function of the Nedd4-Family Ubiquitin Ligase Rsp5. Curr Biol. 2020;30(3):465-79 e5. Epub
870 2020/01/21. doi: 10.1016/j.cub.2019.11.086. PubMed PMID: 31956026; PubMed Central PMCID:
871 PMCPMC7197006.

872 74. Wu N, Zheng B, Shaywitz A, Dagon Y, Tower C, Bellinger G, et al. AMPK-dependent degradation of TXNIP
873 upon energy stress leads to enhanced glucose uptake via GLUT1. Mol Cell. 2013;49(6):1167-75. doi:
874 10.1016/j.molcel.2013.01.035. PubMed PMID: 23453806; PubMed Central PMCID: PMC3615143.
875 75. Castermans D, Somers I, Kriel J, Louwet W, Wera S, Versele M, et al. Glucose-induced posttranslational
876 activation of protein phosphatases PP2A and PP1 in yeast. Cell Res. 2012;22(6):1058-77. doi:
877 10.1038/cr.2012.20. PubMed PMID: 22290422; PubMed Central PMCID: PMCPMC3367521.
878 76. Randez-Gil F, Prieto JA, Sanz P. The expression of a specific 2-deoxyglucose-6P phosphatase prevents
879 catabolite repression mediated by 2-deoxyglucose in yeast. Current genetics. 1995;28(2):101-7. Epub
880 1995/07/01. PubMed PMID: 8590459.
881 77. Momcilovic M, Carlson M. Alterations at dispersed sites cause phosphorylation and activation of SNF1
882 protein kinase during growth on high glucose. J Biol Chem. 2011;286(26):23544-51. Epub 2011/05/13. doi:
883 10.1074/jbc.M111.244111. PubMed PMID: 21561858.
884 78. Mueckler M, Thorens B. The SLC2 (GLUT) family of membrane transporters. Molecular aspects of
885 medicine. 2013;34(2-3):121-38. doi: 10.1016/j.mam.2012.07.001. PubMed PMID: 23506862; PubMed
886 Central PMCID: PMCPMC4104978.
887 79. Bisson LF, Fraenkel DG. Involvement of kinases in glucose and fructose uptake by Saccharomyces
888 cerevisiae. Proc Natl Acad Sci U S A. 1983;80(6):1730-4. Epub 1983/03/01. doi: 10.1073/pnas.80.6.1730.
889 PubMed PMID: 6300872; PubMed Central PMCID: PMCPMC393677.
890 80. Lagunas R. Sugar transport in Saccharomyces cerevisiae. FEMS Microbiol Rev. 1993;10(3-4):229-42. Epub
891 1993/04/01. doi: 10.1016/0378-1097(93)90598-v. PubMed PMID: 8318258.
892 81. Santangelo GM. Glucose signaling in Saccharomyces cerevisiae. Microbiol Mol Biol Rev. 2006;70(1):253-
893 82. doi: 10.1128/MMBR.70.1.253-282.2006. PubMed PMID: 16524925; PubMed Central PMCID:
894 PMCPMC1393250.
895 82. Vega M, Riera A, Fernandez-Cid A, Herrero P, Moreno F. Hexokinase 2 Is an Intracellular Glucose Sensor of
896 Yeast Cells That Maintains the Structure and Activity of Mig1 Protein Repressor Complex. J Biol Chem.
897 2016;291(14):7267-85. doi: 10.1074/jbc.M115.711408. PubMed PMID: 26865637; PubMed Central
898 PMCID: PMCPMC4817161.
899 83. Moreno F, Herrero P. The hexokinase 2-dependent glucose signal transduction pathway of Saccharomyces
900 cerevisiae. FEMS Microbiol Rev. 2002;26(1):83-90. doi: 10.1111/j.1574-6976.2002.tb00600.x. PubMed
901 PMID: 12007644.
902 84. Ma H, Bloom LM, Walsh CT, Botstein D. The residual enzymatic phosphorylation activity of hexokinase II
903 mutants is correlated with glucose repression in Saccharomyces cerevisiae. Mol Cell Biol.
904 1989;9(12):5643-9. doi: 10.1128/mcb.9.12.5643-5649.1989. PubMed PMID: 2685572; PubMed Central
905 PMCID: PMCPMC363735.
906 85. Jayakody LN, Kadowaki M, Tsuge K, Horie K, Suzuki A, Hayashi N, et al. SUMO expression shortens the lag
907 phase of Saccharomyces cerevisiae yeast growth caused by complex interactive effects of major mixed
908 fermentation inhibitors found in hot-compressed water-treated lignocellulosic hydrolysate. Appl
909 Microbiol Biotechnol. 2015;99(1):501-15. doi: 10.1007/s00253-014-6174-9. PubMed PMID: 25359478.
910 86. Brachmann CB, Davies A, Cost GJ, Caputo E, Li J, Hieter P, et al. Designer deletion strains derived from
911 Saccharomyces cerevisiae S288C: a useful set of strains and plasmids for PCR-mediated gene disruption
912 and other applications. Yeast. 1998;14(2):115-32. Epub 1998/03/04. doi: 10.1002/(SICI)1097-
913 0061(19980130)14:2<115::AID-YEA204>3.0.CO;2-2. PubMed PMID: 9483801.
914 87. Hovsepian J, Defenouillere Q, Albanese V, Vachova L, Garcia C, Palkova Z, et al. Multilevel regulation of an
915 alpha-arrestin by glucose depletion controls hexose transporter endocytosis. J Cell Biol.
916 2017;216(6):1811-31. Epub 2017/05/05. doi: 10.1083/jcb.201610094. PubMed PMID: 28468835; PubMed
917 Central PMCID: PMCPMC5461024.
918 88. Huh WK, Falvo JV, Gerke LC, Carroll AS, Howson RW, Weissman JS, et al. Global analysis of protein
919 localization in budding yeast. Nature. 2003;425(6959):686-91. PubMed PMID: 14562095.

920 89. Dohmen RJ, Stappen R, McGrath JP, Forrova H, Kolarov J, Goffeau A, et al. An essential yeast gene
921 encoding a homolog of ubiquitin-activating enzyme. J Biol Chem. 1995;270(30):18099-109. doi:
922 10.1074/jbc.270.30.18099. PubMed PMID: 7629121.

923

Acknowledgments

We thank Agathe Verraes for technical assistance, Olivier Vincent (CSIC, Madrid, Spain) and Michel Becuwe (Harvard University, Cambridge, MA, USA) for sharing reagents and Alexandre Soulard (Université Claude Bernard Lyon 1, Lyon, France) for helpful discussions and critical reading of the manuscript. We also acknowledge the IJM ImagoSeine facility, member of IBiSA and the France-BioImaging infrastructure (https://anr.fr/ProjetIA-10-INBS-0004; ANR-10-INBS-04). This work was supported by grants from the Fondation ARC pour la recherche sur le cancer (https://www.fondation-arc.org, ARCPJA32020060002096 to SL), Université de Paris IDEx (https://u-paris.fr; ANR-18-IDEX-0001, "Emergence en Recherche" RS30J20IDXA1_EMERLEON) and individual fellowships from the Ligue contre le cancer (https://www.ligue-cancer.net; TAZK20115 to CL), the Fondation pour la Recherche Médicale (https://www.frm.org; SPF20150934065 to QD) and the French Ministry for Research and Education (https://www.enseignementsup-recherche.gouv.fr; to AB). The funders had no role in study design, data collection and analysis, decision to publish, or preparation of the manuscript.

Competing interests: The authors have declared that no competing interests exist.

939 # FIGURE LEGENDS

940

941 **Figure 1 - 2DG treatment induces the endocytosis of many plasma membrane proteins, that is mostly**
942 **Rod1-dependent.** (**A**) Cells expressing Hxt2-GFP and Tat1-GFP cells were grown overnight in a glucose-
943 containing medium (exponential phase) and treated with 2DG for 2h30 and observed by fluorescence
944 microscopy. PM: plasma membrane ; V: vacuole. Scale bar: 5 µm. (**B**) Western blot on total protein extracts
945 from Hxt2-GFP- and Tat1-GFP-expressing cells before and after 2DG addition for 2h30, using anti-GFP
946 antibodies. (**C**) Plasma membrane proteins whose localization was examined by fluorescence microscopy
947 before and after 2h30 2DG. When endocytosed, the same proteins were also observed in a *rod1Δ* context to
948 check for Rod1 dependence (NT, not tested). (**D**) Fluorescence microscopy of WT and *rod1Δ* cells expressing
949 the indicated transporters tagged with GFP before and after 2DG treatment for 4h. Scale bar: 5 µm.

950

951 **Figure 2 - Following 2DG treatment, Rod1 is dephosphorylated in a PP1-dependent manner. (A)** Total
952 protein extracts of WT cells expressing either Rod1-Flag or Rod1-KR-Flag were prepared before and after 2DG
953 addition for 10', and immunoblotted using an anti-Flag antibody. Ub: ubiquitylated Rod1, Nat: native Rod1.
954 **(B)** Total protein extracts of WT or *reg1Δ* cells expressing Rod1-Flag were prepared before and after 2DG
955 addition for 10', and immunoblotted using an anti-Flag antibody. Samples were dephosphorylated by CIP
956 where indicated. Ub: ubiquitylated Rod1, Nat: native Rod1, P: phosphorylated Rod1. **(C)** Total protein
957 extracts of WT, *cnb1Δ, slt2Δ, hac1Δ,* or *hog1Δ* expressing Rod1-Flag were prepared before and after 2DG
958 addition for 10', and immunoblotted using an anti-Flag antibody. **(D)** Total protein extract of WT or *snf1Δ*
959 cells expressing Rod1-Flag or Rod1-S12A-Flag were prepared before and after 2DG addition for 10' and
960 immunoblotted using an anti-Flag antibody. **(E)** WT or *rod1Δ* cells expressing the various *ROD1*-Flag
961 constructs were grown in a glucose-containing medium and observed by fluorescence microscopy before and
962 after 2DG treatment for 4h. Scale bar, 5 µm. **(F)** Serial dilutions of cultures of the indicated strains were
963 spotted on SC medium or SC + 0.2% 2DG medium and grown for 4 days at 30°C. **(G)** WT or *snf1Δ* cells
964 expressing Ina1-GFP were grown in a glucose-containing medium and observed by fluorescence microscopy
965 before and after 2DG treatment for 4h. Scale bar, 5 µm.

966

967 **Figure 3 - 2DG causes a fast and temporary dephosphorylation of Snf1 and its substrates through PP1**
968 **activation (A)** Total protein extracts of WT, *reg1Δ* and *snf1Δ* cells were prepared before and after 2DG
969 addition at the indicated concentrations for 10 min and immunoblotted using anti-phospho-AMPK and anti-
970 polyHistidine antibodies. **(B)** *Left*, Total protein extracts of WT, *reg1Δ* and *snf1Δ* cells were prepared before
971 and after 2DG addition for the indicated time and immunoblotted using anti-phospho-AMPK and anti-
972 polyHistidine antibodies. *Right,* quantification of the signals (adjusted *p*-value is indicated, one-way ANOVA).
973 (**C**) Total protein extracts of WT and *reg1Δ* cells expressing Snf1-GFP and Rod1-Flag were prepared before
974 and after 2DG addition for the indicated time and immunoblotted using anti-Flag, anti-phospho-AMPK and
975 anti-GFP antibodies. **(D)** Total protein extracts of WT, *reg1Δ* and *snf1Δ* cells expressing Mig1-Flag were
976 prepared before or after 2DG addition for 10' and 2h and immunoblotted using anti-Flag antibodies.

977

978 **Figure 4 - Hexokinase 2 (Hxk2) is the main 2DG-phosphorylating enzyme *in vivo*** (**A**) Intracellular 2DG6P
979 was assayed enzymatically (see Methods) in WT and *hxk2Δ* cells grown overnight in a glucose-containing
980 medium and treated or not for 15 min with 0.2% 2DG. Values are normalized to the value of the WT / 15 min
981 (n=3 independent experiments ± SEM, *p*value indicated, paired *t*-test) (**B**) 2DG causes a decrease in ATP
982 content as visualized using a FRET ATP biosensor. WT cells expressing the ATP biosensor (WT or mutated
983 version) were grown overnight in a glucose-containing medium and treated with 0.2% 2DG (arrow). The FRET
984 ratio (535/570 nm) was measured over time in a plate reader (see Methods) and is represented as
985 normalized to the t0 value. (*n*=3 independent experiments ± SEM). (**C**) ATP levels were measured as in (B) in

986 WT and *hxk2Δ* cells in response to 2DG. The FRET ratio (535/570 nm) is represented as normalized to the t0
987 value (n=4 independent experiments ± SEM). A paired *t*-test was used to compare WT + 2DG vs *hxk2Δ* + 2DG
988 (*p*-value indicated). (**D**) Total protein extracts of WT and *hxk2Δ* expressing Snf1-GFP and Rod1-Flag were
989 prepared before and after 10' 2DG treatment and immunoblotted using anti-Flag, anti-phospho-AMPK and
990 anti-GFP antibodies. (**E**) WT or *hxk2Δ* cells expressing Ina1-GFP were grown in a glucose-containing medium
991 and observed by fluorescence microscopy before and after 2DG treatment for 4h. Scale bar, 5 µm. (**F**) WT
992 cells expressing Ina1-GFP and transformed with an empty plasmid, or with plasmids allowing the
993 overexpression of *DOG2* or its catalytic mutant *DOG2-DDAA* were grown in a glucose-containing medium and
994 observed by fluorescence microscopy before and after 2DG treatment for 4h. Scale bar, 5 µm.
995
996 **Figure 5- Low affinity glucose transporters are required for the resistance of the *rod1Δ* mutant to 2DG**
997 (**A**) Beta-galactosidase assays of WT and *rod1Δ* cells expressing *LacZ* under the control of the p*DOG1* or
998 p*DOG2* promoters, before and after 2DG treatments for 4h (+- SEM, n=3 independent experiments, *t*-test).
999 A.U., arbitrary units. (**B-D**) Serial dilutions of cultures of the indicated strains were spotted on SC medium or
1000 SC + 0.2% 2DG medium and grown for 4 days at 30°C.
1001

1002
1003 **Figure 6- The maintenance of glucose transporters in the *rod1Δ* mutant promotes 2DG resistance by**
1004 **increasing glucose uptake and limiting 2DG toxicity** (**A**) Serial dilutions of cultures of the indicated strains
1005 were spotted on SC medium or SC + 0.2% 2DG medium and grown for 4 days at 30°C. (**B**) Intracellular 2DG6P
1006 was assayed enzymatically in WT and *rod1Δ* cells grown overnight in a glucose-containing medium, treated
1007 for 2h with 0.2% 2DG, and then transferred into a 2DG-free glucose-containing medium ("chase"). Values are
1008 normalized to the value of the WT / 2h (n=4 independent experiments ± SEM, paired *t*-test, *p*-value
1009 indicated). (**C**) 2DG6P content was assayed from WT cells as in (**B**) after 15 min and 2h treatment with 0.2%
1010 2DG n=4 independent experiments ± SEM, paired *t*-test, *p*-value indicated). (**D**) Intracellular 2DG6P was
1011 assayed enzymatically in WT, *hxt3Δ, rod1Δ* and *rod1Δ hxt3Δ* cells as in (**B**). Values are normalized to the value
1012 of the WT / 2h (n=3 independent experiments ± SEM, paired *t*-test, *p*-value indicated).(**E**) Intracellular
1013 glucose measurement using a FRET-based glucose biosensor (representative experiment). Cells were grown
1014 overnight in glucose medium (exponential phase), treated for 4h with 0.2% 2DG, and transferred in a
1015 glucose-free buffer. Fluorescence at 485 and 528 nm was measured every 90 sec in a plate reader before and
1016 after glucose addition (2%) (see Methods) and the FRET ratio (485/528 nm) is indicated over time. (**F**)
1017 Intracellular glucose was evaluated as in (**D**) at 2000 sec across *n*=5 independent experiments (± SEM, paired
1018 *t*-test) and is represented as normalized to the "before glucose" value. (**G**) Serial dilutions of cultures of the
1019 indicated strains were spotted on SC medium or SC + 0,1% 2DG medium and grown for 4 days at 30°C.
1020

1021 **Figure 7 - Hypothetical model for a role of hexose transporters in 2DG detoxification.** Treatment of cells
1022 with 2DG triggers the accumulation of intracellular 2DG6P. This activates stress-signaling pathways such as
1023 cell-wall integrity signaling (CWI) or the unfolded protein response (UPR), converging onto *DOG2* expression
1024 (1) [20]. On the other hand, 2DG6P elicits a fast PP1 activation (2) which causes AMPK inhibition and, either
1025 directly or indirectly, Rod1 dephosphorylation. By the time Dog2 is induced and begins to dephosphorylate
1026 2DG6P (3), Rod1 has already triggered the endocytosis of many plasma membrane proteins (4), including
1027 that of low affinity glucose transporters. This may prevent 2DG exit and detoxification but also affect cell
1028 survival by reducing glucose import (5).

A.

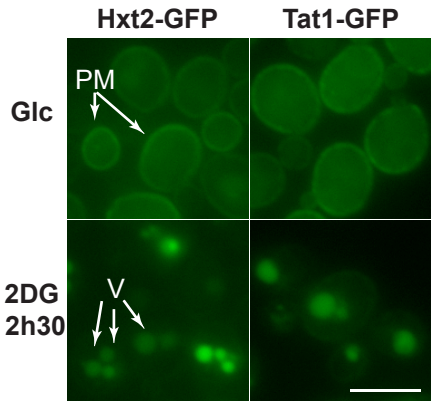

B.

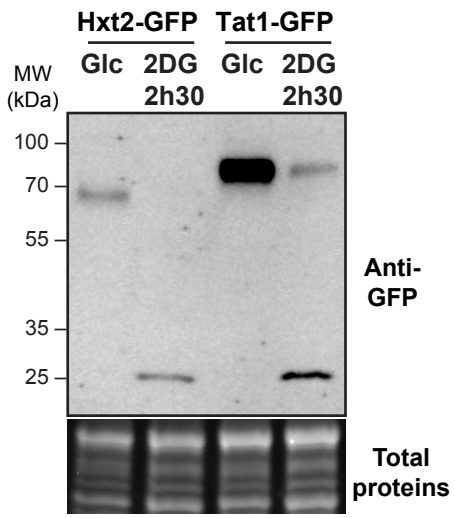

C.

Name	Function	Endocy-tosis ?	Rod1-depdt?
Hxt1	Glucose transporter (low aff)	Yes	Yes
Hxt3	Glucose transporter (low aff)	Yes	Yes
Hxt2	Glucose transporter (med/high aff)	Yes	Yes
Hxt4	Glucose transporter (med/high aff)	Yes	Yes
Qdr3	Multidrug transporter (MFS type)	Yes	Yes
Pdr12	Multidrug transporter (ABC type)	Yes	Yes
Vht1	Biotin transporter	Yes	No
Fui1	Uridine permease	Yes	Yes
Tat1	Tryptophan permease	Yes	Yes
Lyp1	Lysine permease	Yes	No
Can1	Arginine permease	Yes	No
Itr1	Inositol transporter	Yes	Yes
Bap2	Leucine permease	Yes	NT
Ste2	GPCR (α-factor pheromone)	Yes	No
Ina1	Unknown	Yes	Yes
Slg1/Wsc1	Cell wall stress sensor	No	-
Wsc2	Cell wall stress sensor	No	-
Wsc3	Cell wall stress sensor	No	-
Mid2	Cell wall stress sensor	No	-
Fps1	Aquaglyceroporin	No	-

D.

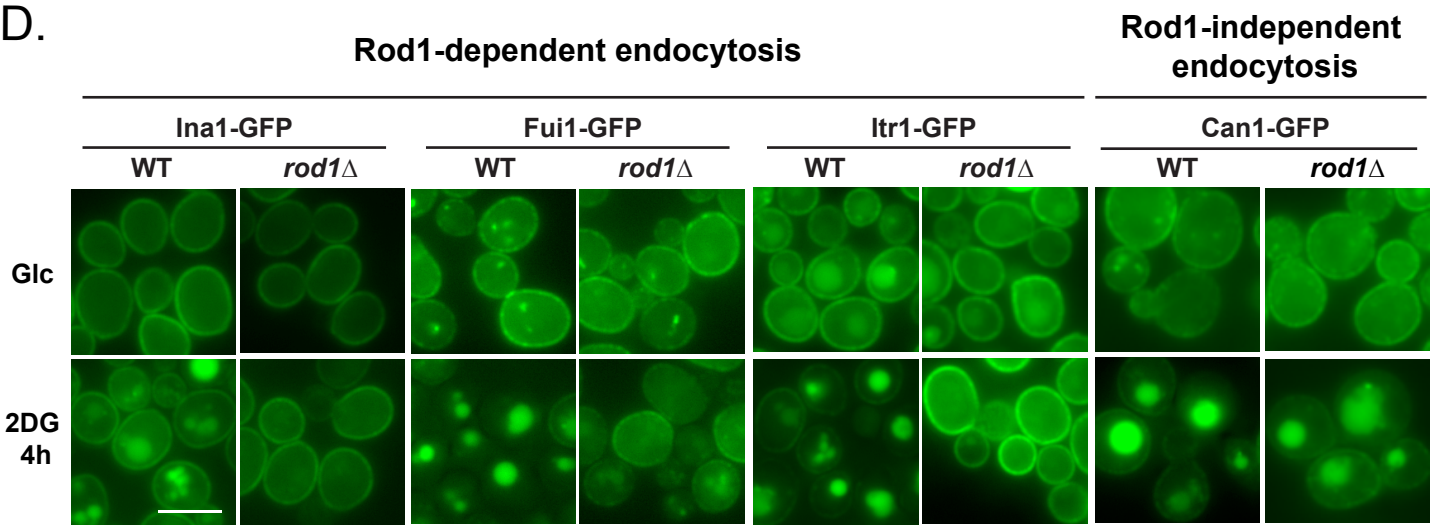

Laussel et al. Fig 1

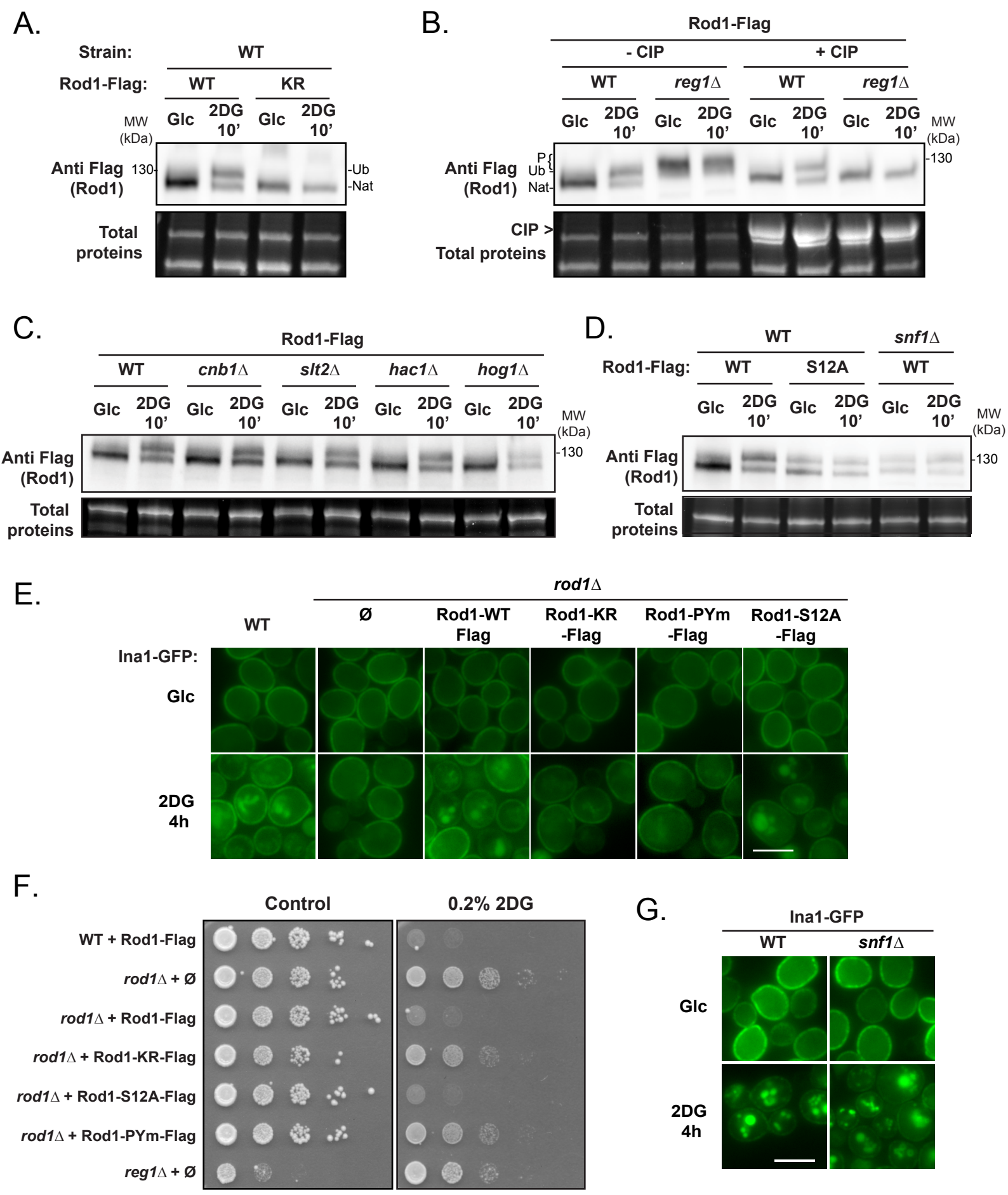

Laussel et al. Fig 2

A.

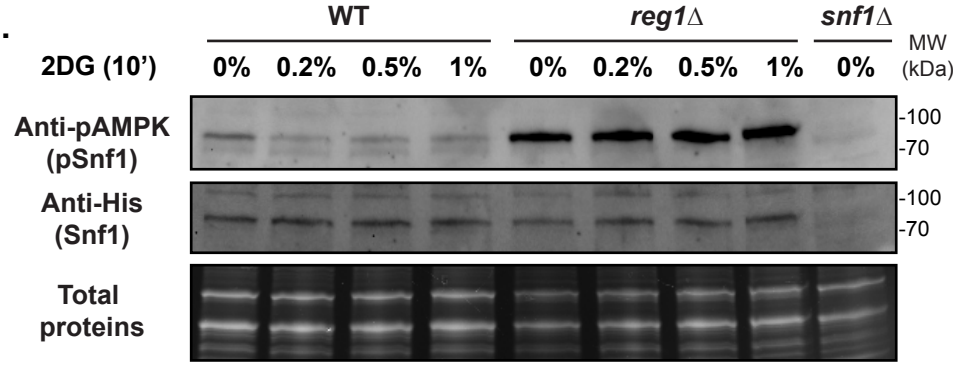

B.

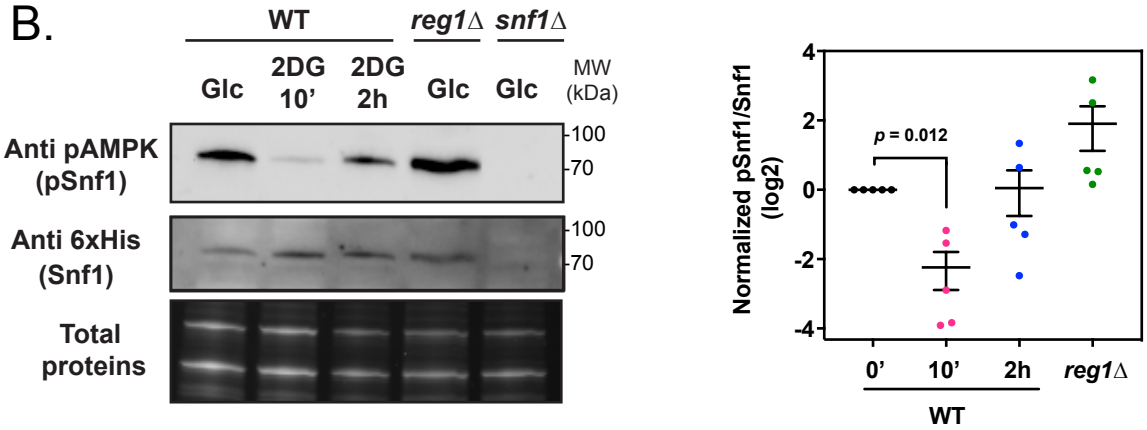

C.

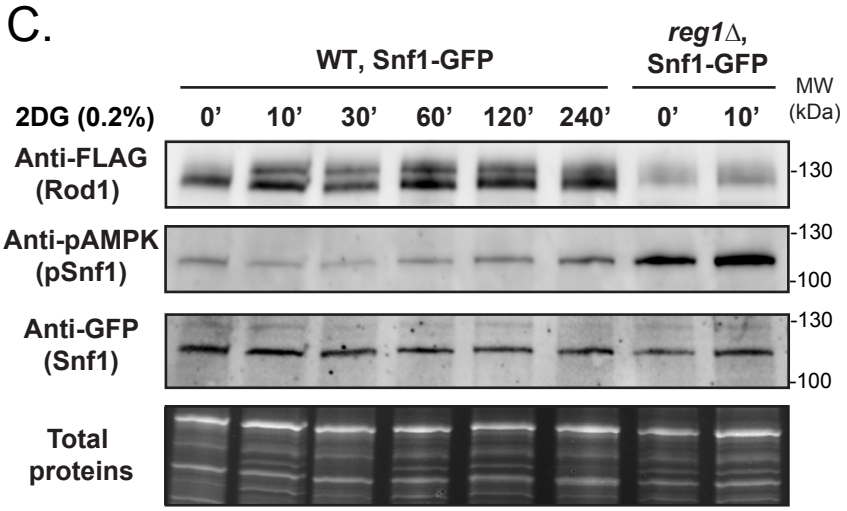

D.

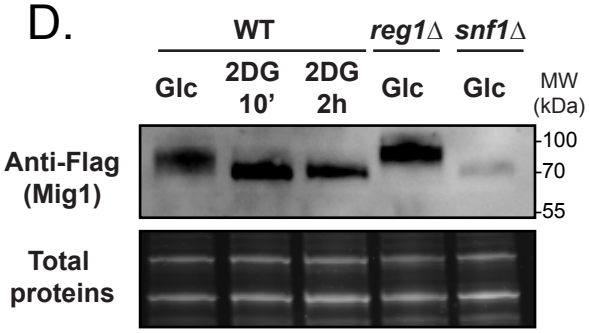

Laussel et al. Fig 3

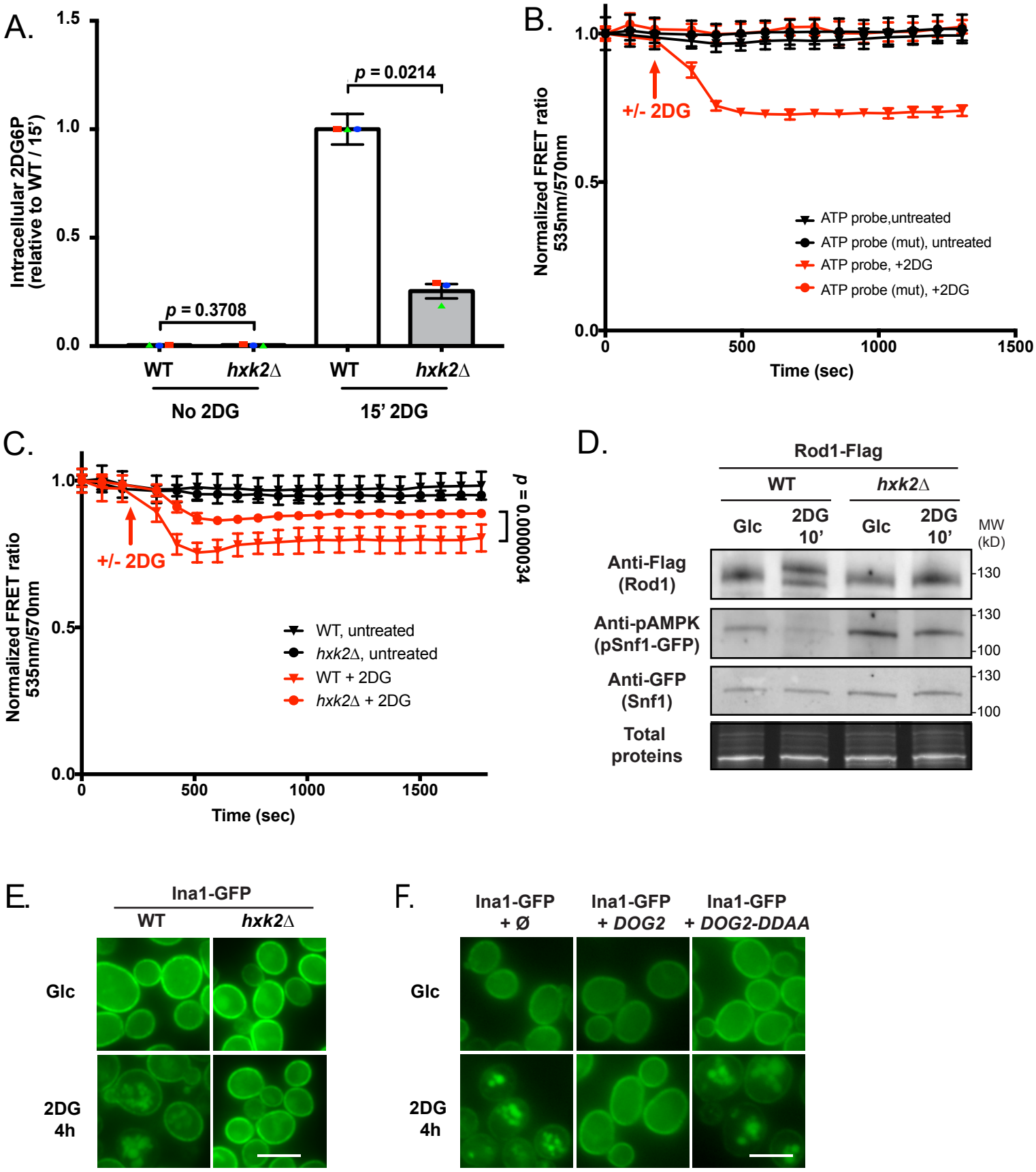

Laussel et al. Fig 4

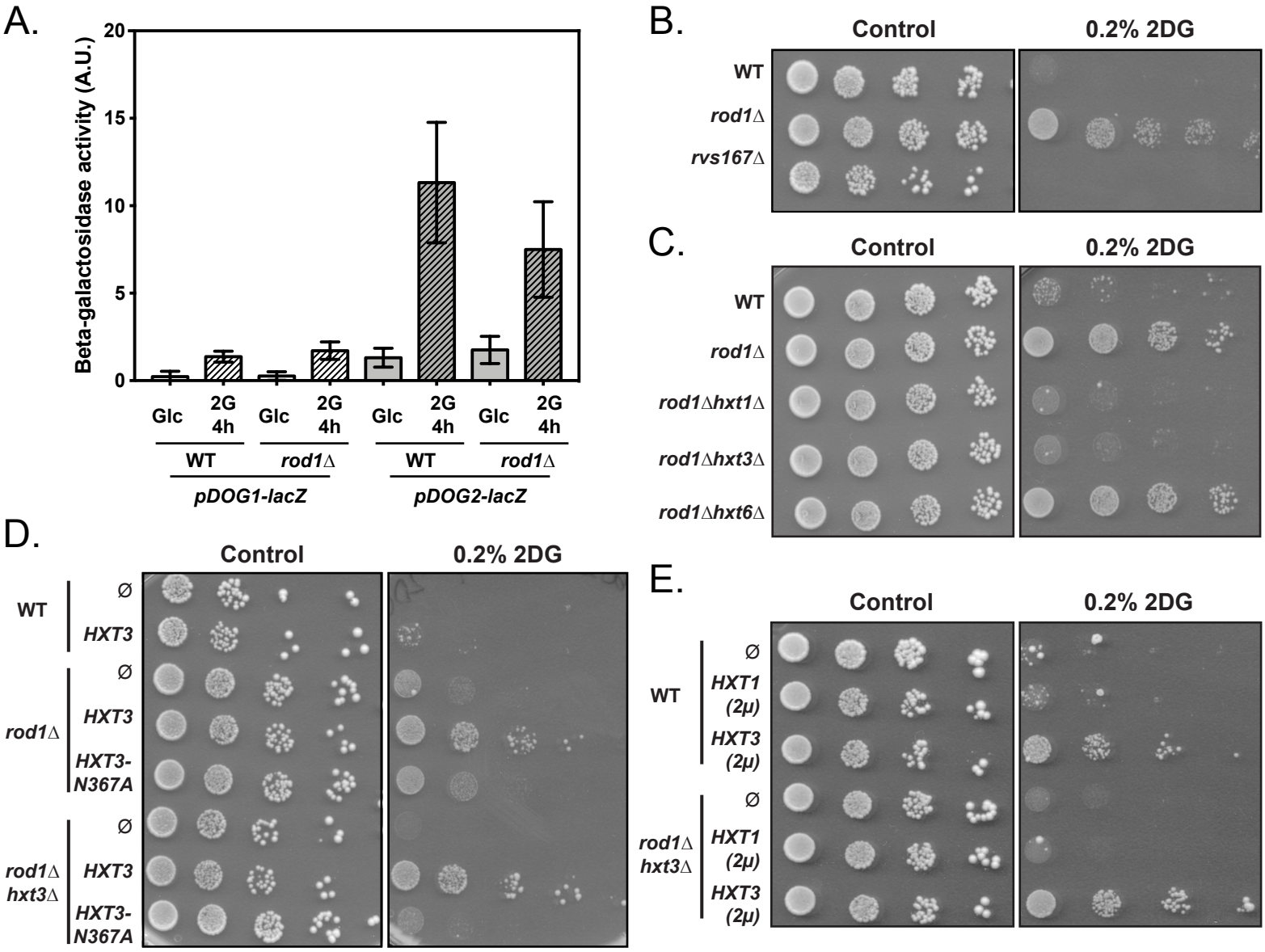

Laussel et al. Fig 5

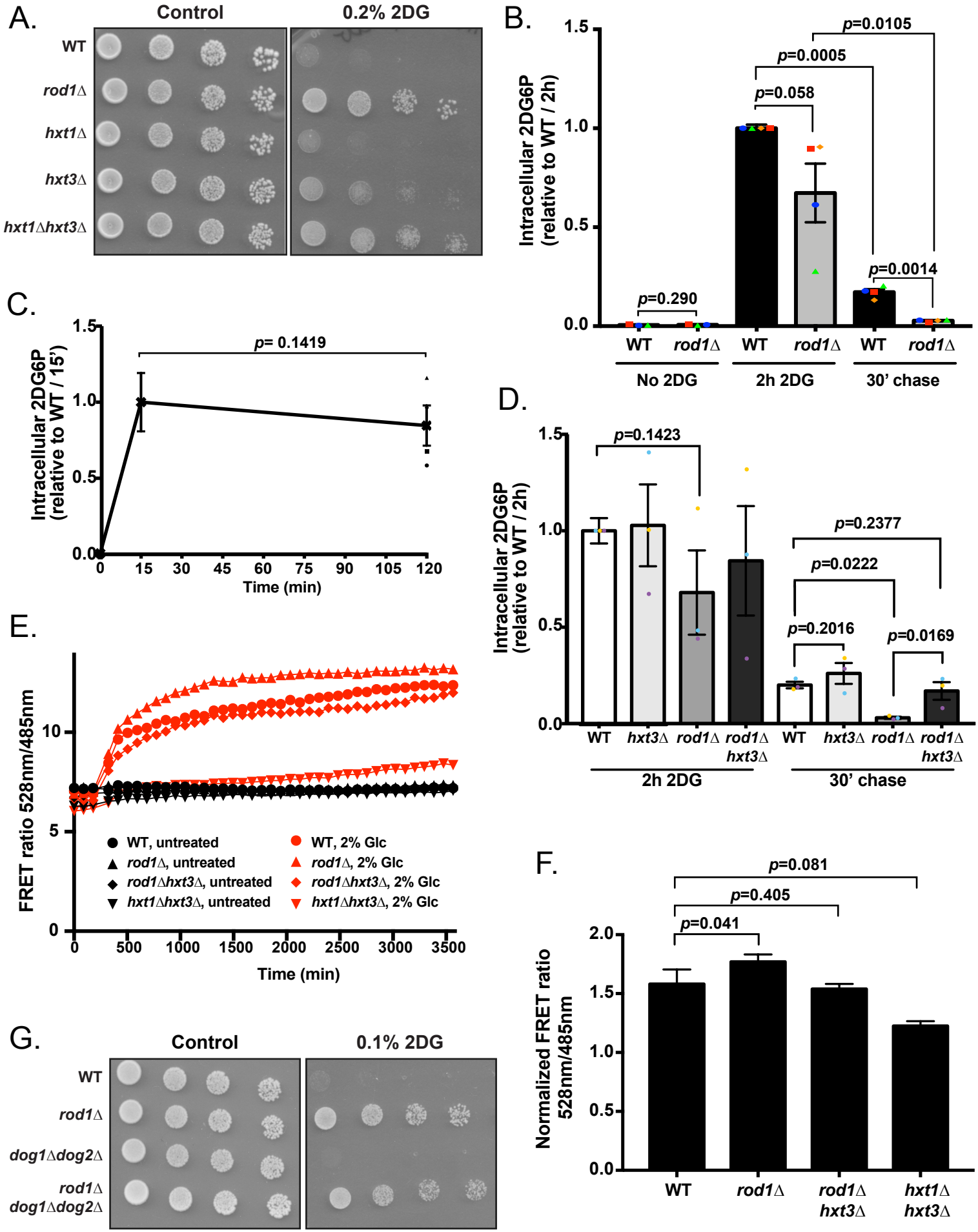

Laussel et al. Fig 6

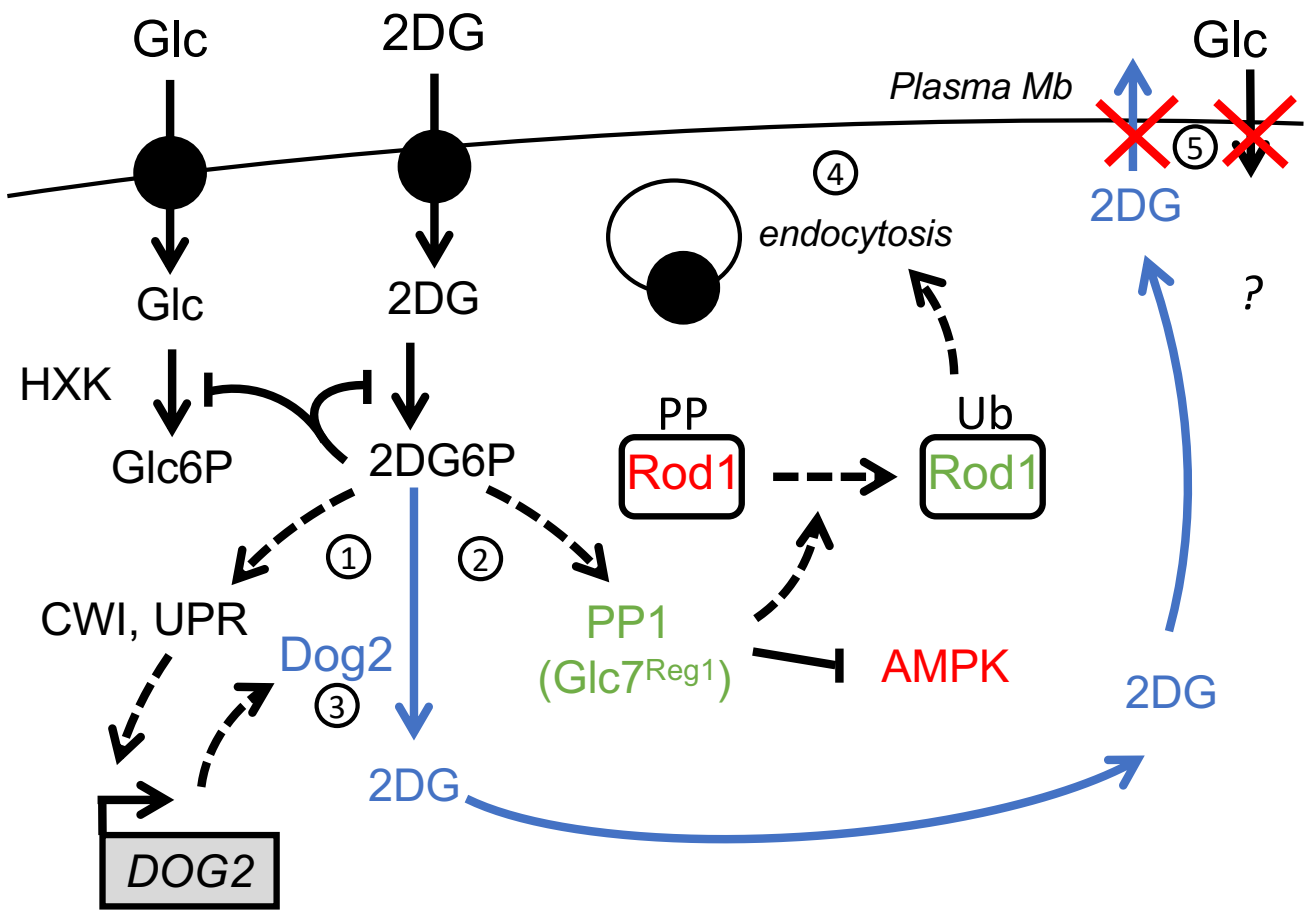

Laussel et al. Figure 7.

A.

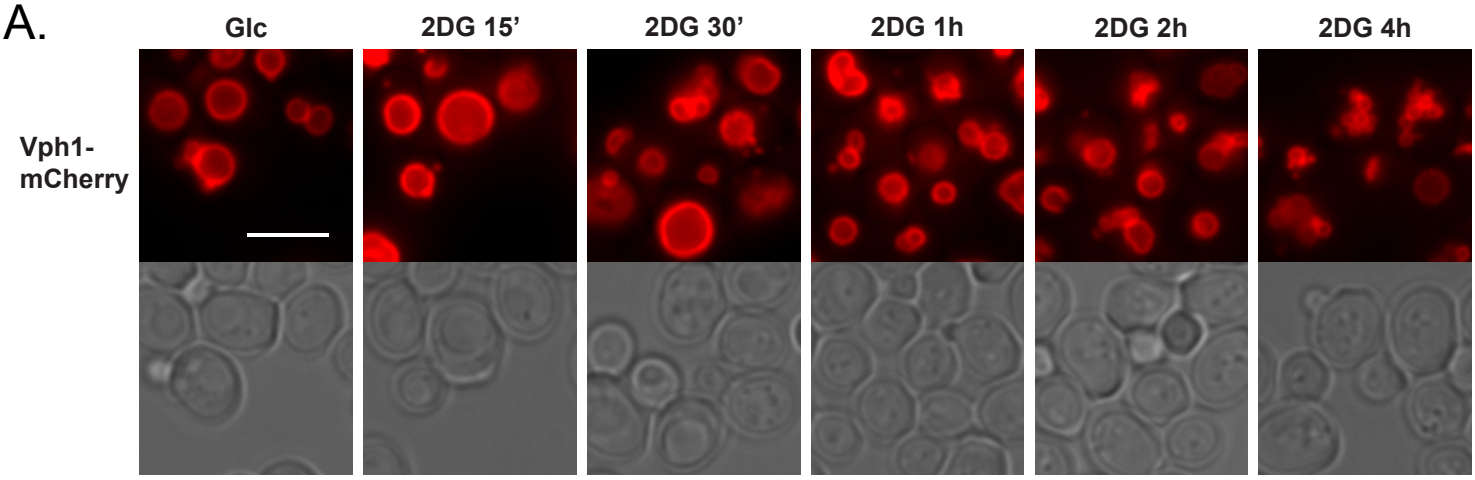

B.

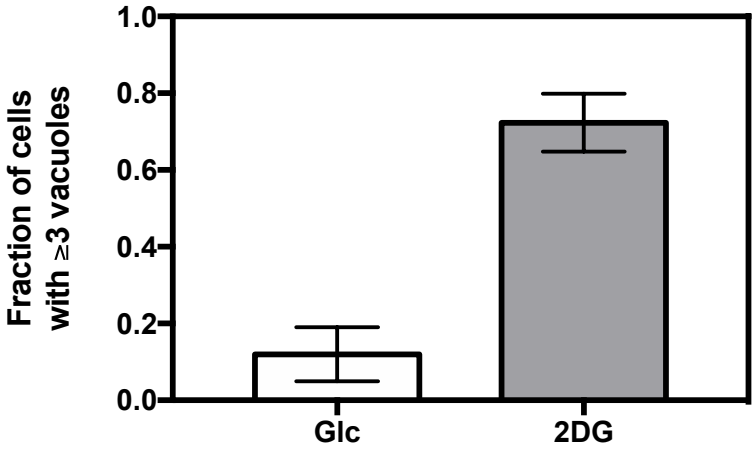

Laussel et al. Fig S1

Endocytosis in response to 2DG

Rod1-dependent

Hxt1-GFP | Hxt3-GFP | Itr1-GFP | Hxt4-GFP

WT | *rod1*Δ

Glc

2DG 4h

Qdr3-GFP | Pdr12-GFP | Hxt2-GFP

WT | *rod1*Δ

Glc

2DG 4h

Rod1-independent

Ste2-GFP | Lyp1-GFP | Vht1-GFP

WT | *rod1*Δ

Glc

2DG 4h

Not tested

Bap2-GFP

WT

Glc

2DG 4h

No endocytosis in response to 2DG

Slg1-GFP | Wsc2-GFP | Wsc3-GFP | Mid2-GFP | Fps1-GFP

Glc

2DG 4h

Laussel et al. Figure S2

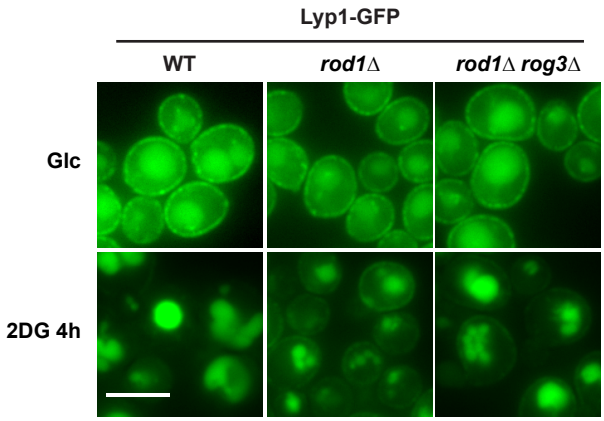

Laussel et al. Figure S3

A.

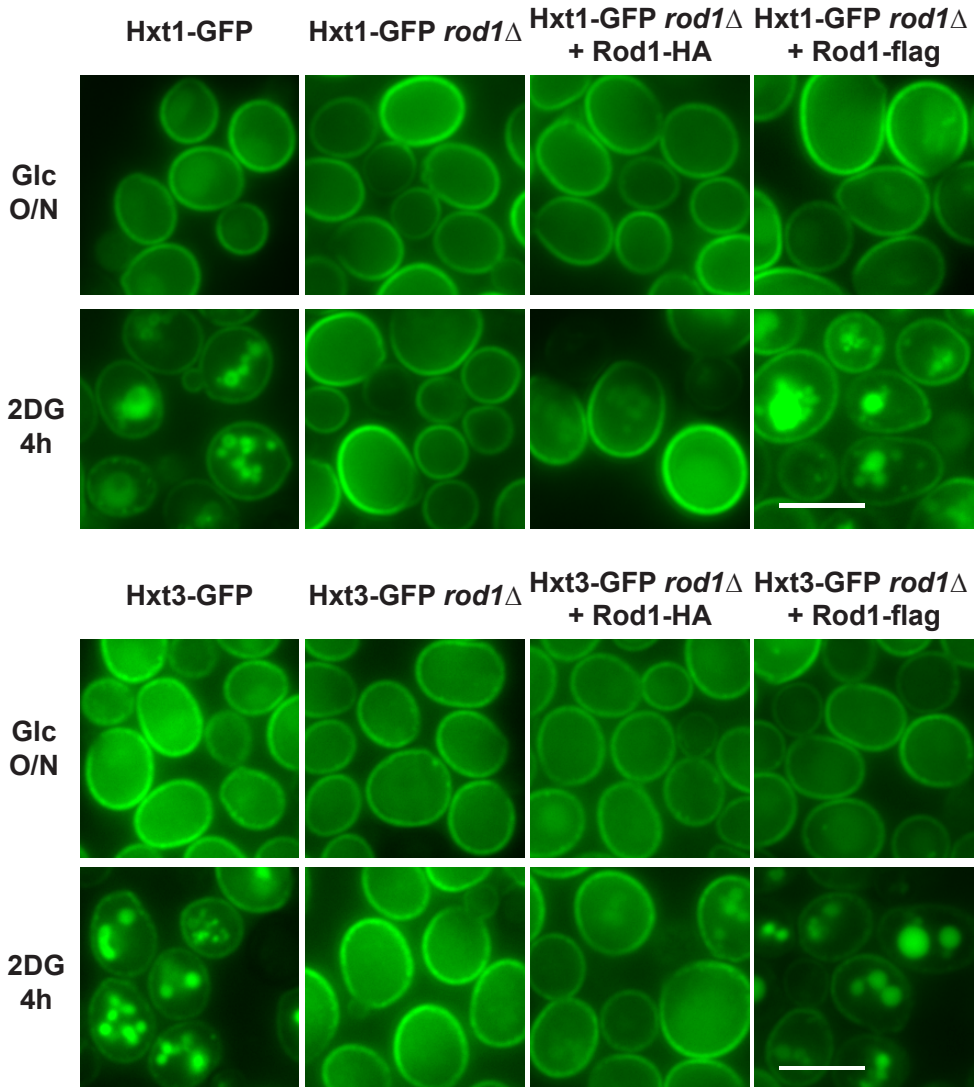

B.

Strain	*LEU2* plasmid	*URA3* plasmid
WT	Ø	Ø
*reg1*Δ	Ø	Ø
*rod1*Δ	Ø	Ø
*rod1*Δ	Rod1-3HA	Ø
*rod1*Δ	Ø	Rod1-GFP
*rod1*Δ	Ø	Rod1-Flag

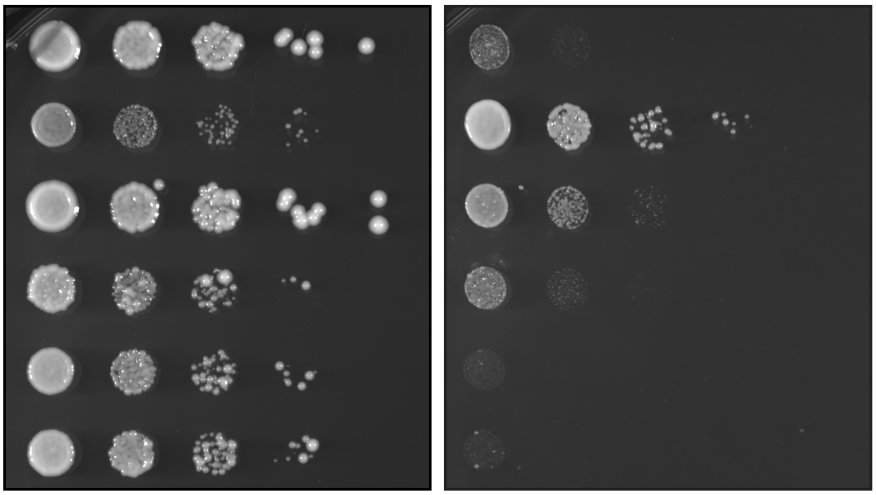

Laussel et al. Figure S4

A.

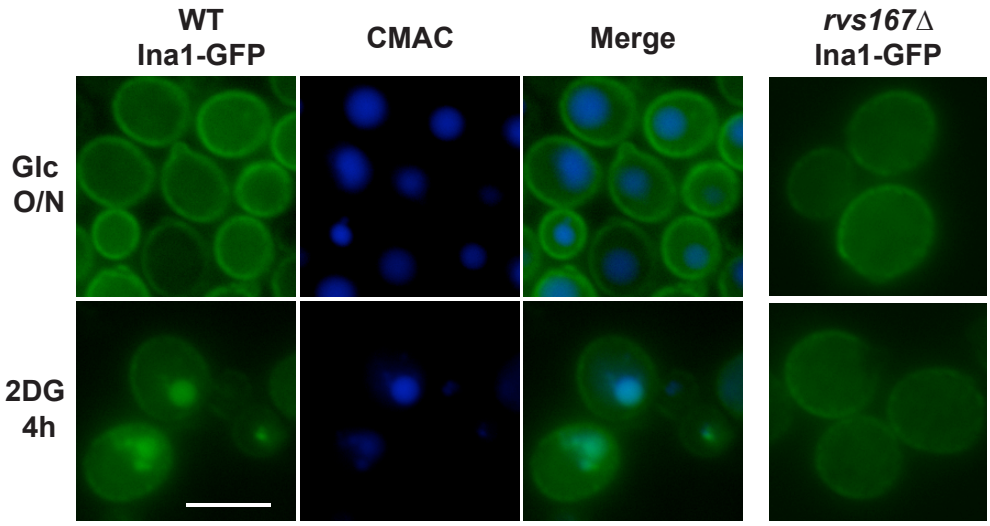

B.

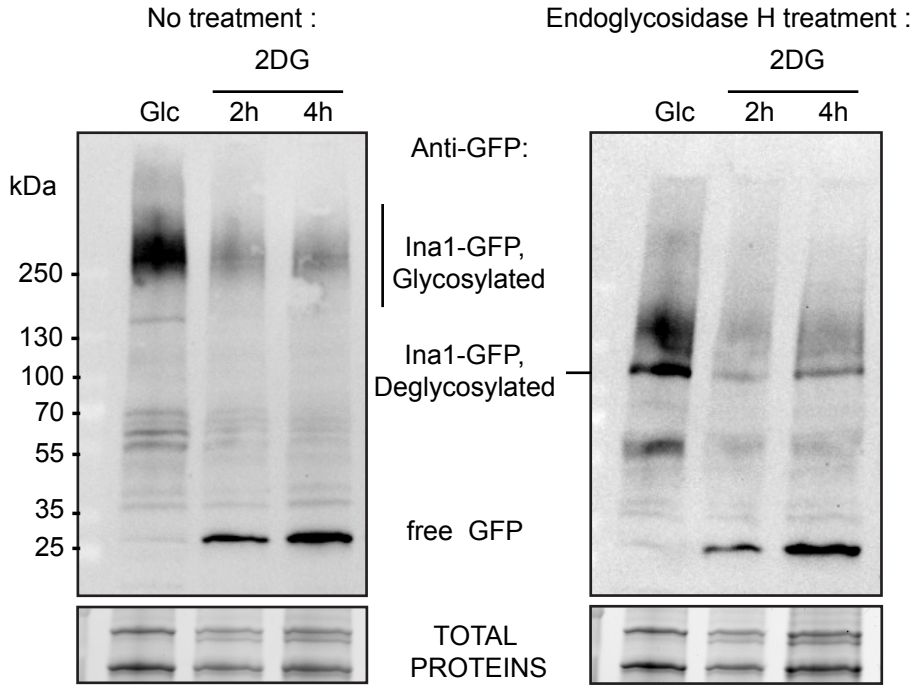

Laussel et al. Fig S5

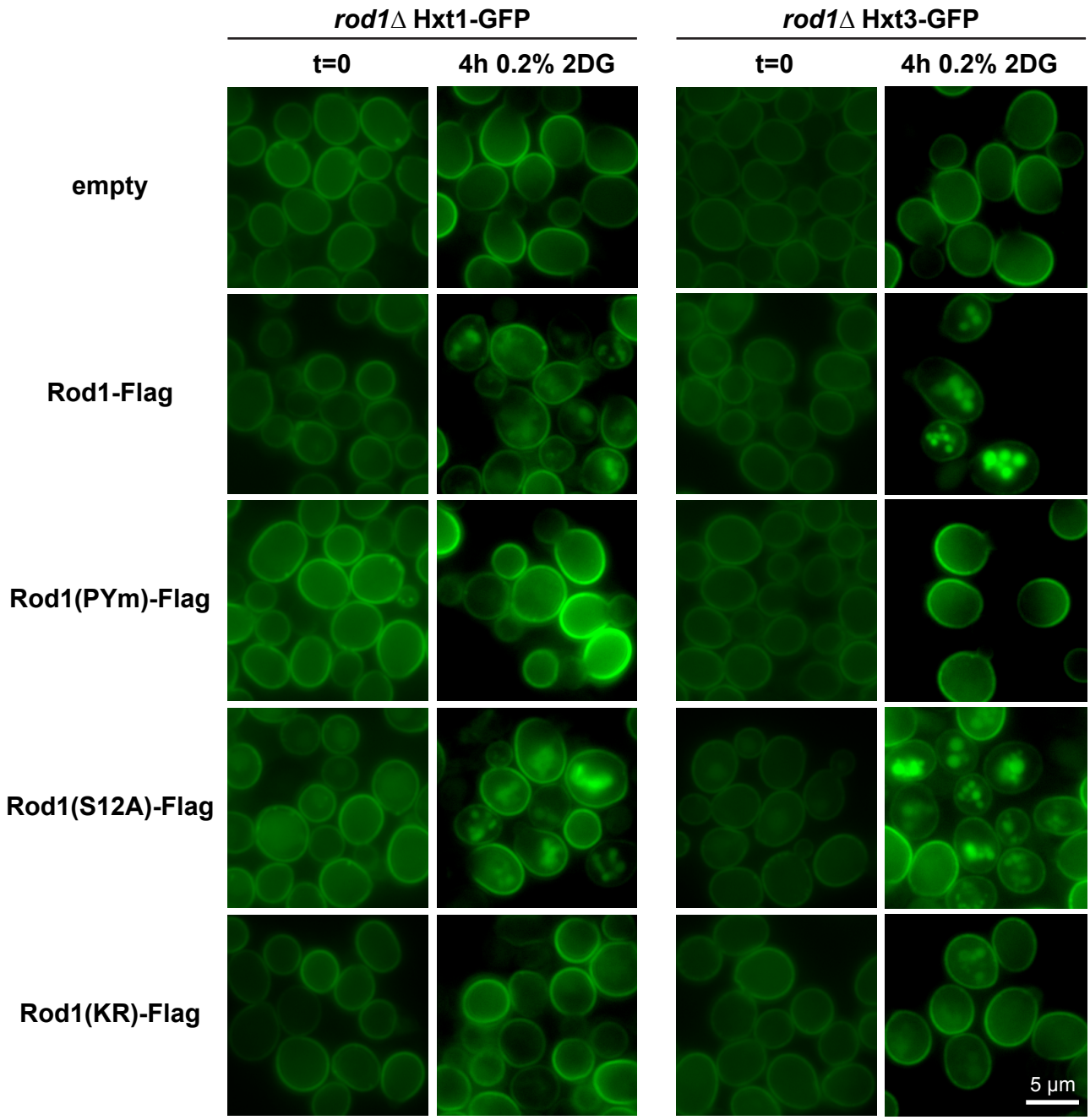

Laussel et al. Figure S6

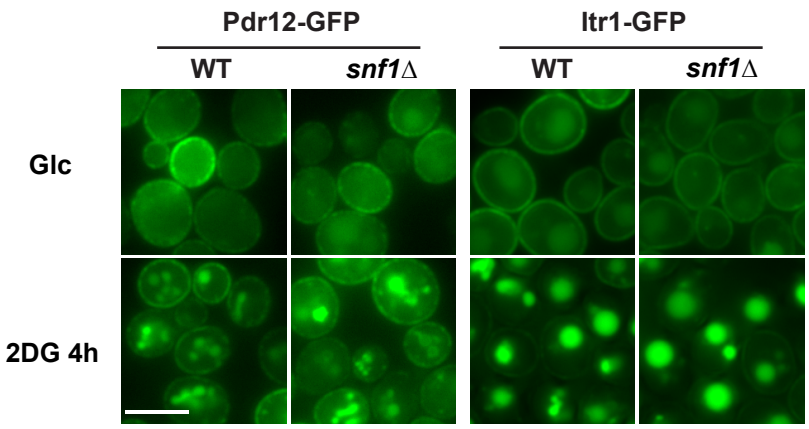

Laussel et al. Figure S7

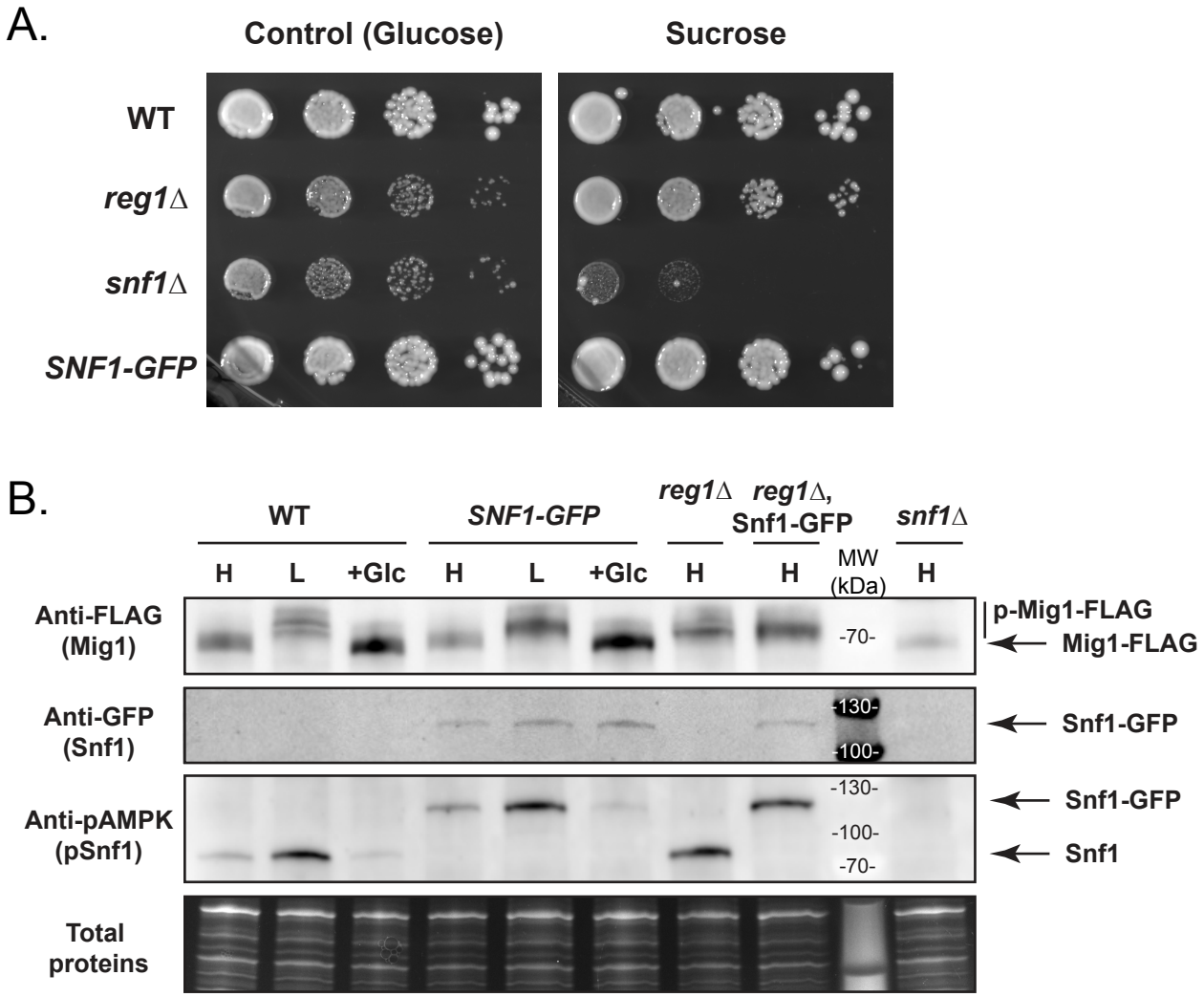

Laussel et al. Figure S8

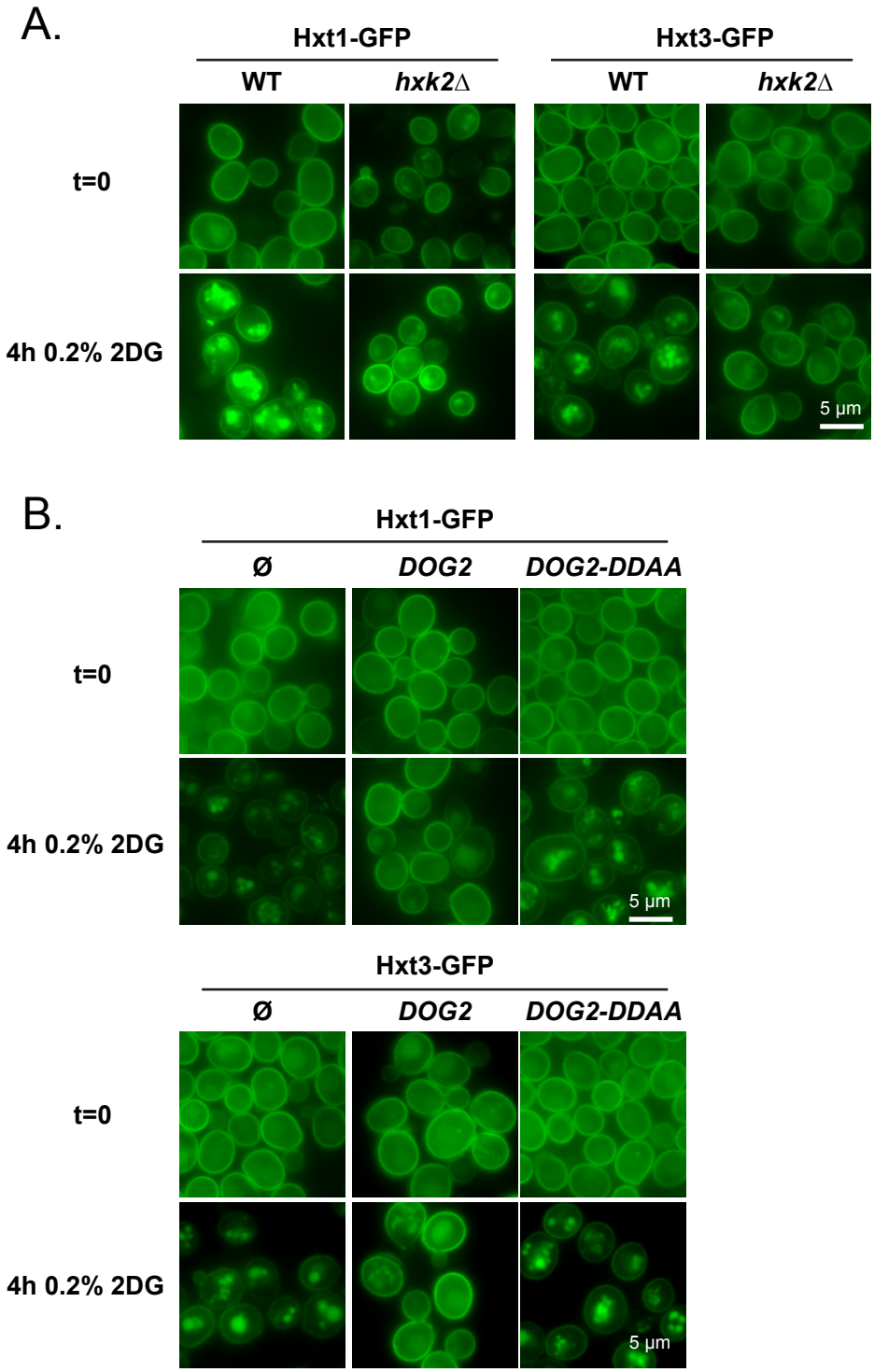

Laussel et al. Figure S9